

TIMING OBSERVATIONS OF 27 PULSARS AT THE PUSHCHINO OBSERVATORY FROM 1978 to 2012

T. V. Shabanova, V. D. Pugachev, and K. A. Lapaev

*Pushchino Radio Astronomy Observatory, Astro Space Center, P. N. Lebedev Physical
Institute, Russian Academy of Sciences, 142290 Pushchino, Russia*

tvsh@prao.ru

ABSTRACT

We present results from timing observations of 27 pulsars made at the Pushchino Observatory over 33.5 yr between 1978 July and 2012 February. We also analyze archival Jet Propulsion Laboratory data of 10 pulsars to extend individual data span to 43.5 yr. We detected a new phenomenon in the timing behavior of two pulsars, B0823+26 and B1929+10, that demonstrates a rapid change of pulsar rotation parameters such that the sign of the second derivative $\ddot{\nu}$ is reversed. An analysis of the $\ddot{\nu}$ changes showed that this process can be considered as a modulation process in $\ddot{\nu}$. We showed that the process of rapidly changing of pulsar rotation parameters represents a new type of rotational irregularity that, together with three other types of rotational irregularities (discrete glitches, slow glitches and quasi-periodic oscillations), forms a large-scale structure of timing noise. These effects are all the cause of the deviation of the timing behavior of most ordinary pulsars from a simple ν , $\dot{\nu}$ spin-down model. We found that all four types of observed rotational irregularities have evolving nature. Irregularities in pulsar rotation rate pass through three evolutionary stages that show that a certain type of rotational irregularity can occur only at a certain stage of pulsar rotation evolution. The age boundaries between different evolutionary stages are indistinct and diffusive. This fact is because different pulsars having similar properties evolve along different paths. The evolutionary scenario of the occurrence of rotational irregularities explains well many of the observed properties of pulsar rotation.

Subject headings: pulsars: general – stars: neutron – stars: rotation

1. Introduction

According to theoretical suggestions, a regular secular decrease in the pulsar rotation frequency can be described by the relation $\dot{\nu} \propto -\nu^n$, where n is the braking index (Manchester & Taylor 1977). For the vacuum dipole model, when the secular spin-down is due to magnetic dipole radiation, $n = 3$. The direct way of defining the braking index, $n = \nu\ddot{\nu}/\dot{\nu}^2$, is based on a measurement of the second derivative $\ddot{\nu}$ from the pulsar observations. The early timing observations showed that the rotation rate of many pulsars is subject to irregularities such as glitches (discrete jumps in the rotation rate) and timing noise (variations in the pulse arrival times). These irregularities disturb the steady secular spin down and hinder a measurement of the deterministic values of $\dot{\nu}$. For ordinary pulsars, the values of $\ddot{\nu}$ due to slowdown are very small in comparison to the measurement uncertainties and a rotation phase should be well described by a simple ν , $\dot{\nu}$ spin-down model. In actuality, most ordinary pulsars show significant deviations from a simple spin-down model. An analysis of timing noise for these pulsars has shown that these deviations are due to a random, continuous wandering of the pulse phase that produces long-term cubic polynomial components in the timing residuals. These components lead to the large observed $\ddot{\nu}$ values and accordingly to anomalously high values of the braking indices (Cordes & Helfand 1980; Gullahorn & Rankin 1982; Cordes & Downs 1985).

The properties of timing noise have been studied by numerous authors over the past 40 yr (Boynton et al. 1972; Helfand et al. 1980; Cordes & Helfand 1980; Gullahorn & Rankin 1982; Cordes & Downs 1985; Arzoumanian et al. 1994; D’Alessandro et al. 1995; Lyne 1996; Baykal et al. 1999; Hobbs et al. 2004, 2010). It has been established that timing noise is widespread in pulsars. The strength of the timing noise is correlated with the period derivative and is quantified by a parameter based on the non-zero second derivative $\ddot{\nu}$. In fact, the observed $\ddot{\nu}$ value is the measure of timing noise in pulsars (Cordes & Downs 1985; Arzoumanian et al. 1994; Hobbs et al. 2010). It is widely believed that timing noise can be explained by random fluctuations in the pulsar rotation rate. A description of timing noise is constructed in the context of physical models that are based on noise-like processes.

Important results were recently obtained by Hobbs et al. (2010) who presented a detailed study of the timing behavior of 366 pulsars observed at the Jodrell Bank Observatory (JBO) over a long time span of 36 yr. It was shown that a variety of different structures visible in the timing residuals can be classified into groups. Out of a sample of 366 pulsars, approximately 37% pulsars have timing residuals where noise-like variations dominate, about 36% pulsars have residuals where cubic structures with both signs dominate, and the remaining 27% of pulsars show more complex structures. Hobbs et al. (2010) pay attention to the necessity of using long data spans to analyze the timing residuals, as otherwise the

structure of the residuals will depend on the length of the data span analyzed. Hobbs et al. (2010) discussed in detail the problems that are related to timing noise and the large values of the measured second derivatives $\ddot{\nu}$ in pulsars, and paid attention to the important properties of timing noise. First, there is a large anti-correlation between the amount of timing noise and characteristic age. Pulsars with smaller characteristic ages have more timing noise than older pulsars. Second, there is a relation between the signature of timing residuals and characteristic age: the timing residuals observed for the pulsars with the smaller characteristic ages exhibit mainly cubic signatures, whereas the timing residuals seen for older pulsars have quasi-periodic characteristics. The main conclusion of this paper is that the timing residuals cannot be explained by the models that are based on noise-like processes because such models are not consistent with observations over long time scales.

In this paper, we analyze a 33.5 yr period of pulsar timing observations made at the Pushchino Radio Astronomy Observatory (PRAO) between 1978 and 2012. The PRAO data sets for 10 pulsars that are in common with the Jet Propulsion Laboratory (JPL) sample were combined with the archival JPL data spanning the years 1968–1983 (Downs & Reichley 1983; Downs & Krause-Polstorff 1986). This procedure extends the individual data spans for some pulsars up to 43.5 yr. The common pulsars are B0329+54, B0823+26, B0919+06, B0950+08, B1133+16, B1642–03, B1737+13, B1929+10, B2016+28, and B2217+47. The combined data set for PSR B1642–03 includes also the JBO data collected over the interval 1981–1999 taken from an earlier paper (Shabanova et al. 2001). The data set for PSR B1822–09 includes the Hartebeesthoek Radio Astronomy Observatory data collected over the interval 1985–1998 taken from a published paper (Shabanova & Urama 2000).

While our sample of 27 pulsars is small, these objects nevertheless reflect the properties of a large number of pulsars. Figure 1 shows a histogram of the characteristic ages of known pulsars based on the ATNF Pulsar Catalogue (Manchester et al. 2005)¹. The 27 studied pulsars have ages ranging from 2.3×10^5 to 1.2×10^8 yr; this interval is marked by the horizontal line. More than 80% of the global pulsar population has ages within this range.

On the basis of a detailed analysis of the timing residuals of these pulsars, we obtained the following results. First, we detected a new phenomenon in the timing behavior of two pulsars, B0823+26 and B1929+10, that demonstrates a rapid change of pulsar rotation parameters in which the sign of $\ddot{\nu}$ is reversed. This phenomenon may be interpreted as a modulation process that changes the sign of $\ddot{\nu}$. The second result is that we showed that a long-term structure of timing noise is produced by four types of rotational irregularities that have an evolving nature and form three evolutionary stages in pulsar rotation. According to

¹<http://www.atnf.csiro.au/research/pulsar/psrcat>

the evolutionary scenario, certain types of rotational irregularities can only occur at certain stages of pulsar rotation evolution.

2. Observations and Timing Analysis

Pulsar timing observations were carried out at the Pushchino Observatory from 1978 July to 2012 February with a four-year gap between 1987 and 1990. The observations were made with the BSA radiotelescope, which operated at frequencies close to 102.7 MHz until 1998 May and around 111.3 MHz since 1998 November. A 64-channel radiometer with a channel bandwidth of 20 kHz was used for the pulsar observations. The data were sampled at intervals of 2.56 or 1.28 ms. The BSA radiotelescope, made up of a linearly polarized transit antenna with a beam size of about $(3.5/\cos \delta)$ min, provided the duration of the observing session ranging from 3 to 11 minutes at different pulsar declinations δ . During this time, individual pulses were summed synchronously with a predicted topocentric pulsar period to form the mean pulse profile in each 20 kHz channel. After dispersion removal, all the channel profiles were summed to produce a mean pulse profile for the given observing session. The topocentric arrival times of the pulses for each observing session were calculated by cross-correlating the mean pulse profile with a standard low-noise template. The parameters of the PRAO timing observations are listed in Table 1. In column order, the table lists the pulsar’s J2000 and B1950 names, the MJD range of the PRAO observations, the number of pulse time of arrival (TOA), the mean measurement error for each observing session, and the dispersion measure (DM) parameter. The references in the last column mark the DM value that provided the best adjustment between the two sets of the timing residuals obtained for each pulsar at the two observing frequencies of 102.7 MHz (until 1998 May) and 111.3 MHz (since 1998 November) in the PRAO observations.

Timing parameters were determined using the program TEMPO ² and the JPL DE200 ephemeris. The topocentric arrival times collected at the PRAO and the geocentric arrival times obtained from the archival JPL timing data were all corrected to the barycenter of the solar system at infinite frequency. The position and the proper motion required for this correction were taken from Hobbs et al. (2004) and were held constant during the fitting procedure. The positions of most of the pulsars from our sample do not require correction since their residuals (defined as the observed minus predicted arrival times) obtained after the fitting procedure did not show a sinusoid with a period of 1 yr within the precision of the measurements. Position corrections were needed for pulsars B1508+55, B2020+28, and

²<http://www.atnf.csiro.au/research/pulsar/tempo>

B2224+65, which are fast moving pulsars, but a timing solution did not provide improved positions for these pulsars because of the large timing noise. As the timing behavior of these pulsars was analyzed over a long interval, the presence of a weak annual sine wave at the end of this interval does not affect the large-scale structure of the timing residuals.

The regular change of pulsar’s rotation frequency with time is well described by a polynomial including several frequency derivatives (Manchester & Taylor 1977). In accordance with a Taylor expansion, the pulse phase φ at the barycentric arrival time t is expressed as:

$$\varphi(t) = \varphi_0 + \nu(t - t_0) + \dot{\nu}(t - t_0)^2/2 + \ddot{\nu}(t - t_0)^3/6\dots, \quad (1)$$

where φ_0 , ν , $\dot{\nu}$, and $\ddot{\nu}$ are the pulse phase, rotation frequency, and the first and second frequency derivative at some reference time t_0 , respectively. The timing residuals, obtained as the differences between the observed times and the times predicted by a best-fit model, are used for the analysis of the rotation behavior of the pulsar.

In order to study the time changes in a pulsar’s rotation frequency in more detail, we show the plots of the timing residuals together with the plots of the frequency residuals $\Delta\nu$ relative to the different timing models. At first, the timing residuals are calculated relative to a second-order polynomial, including the mean rotation parameters ν and $\dot{\nu}$ defined over the whole data span. The corresponding frequency residuals $\Delta\nu$ are obtained as a result of calculating the parameters ν and $\dot{\nu}$ from the local fits, performed to the pulse arrival times over intervals from 150 to 300 days. The $\Delta\nu$ residuals are given relative to the mean parameters ν and $\dot{\nu}$ and are referenced to the first point of each interval. Next, the timing and frequency residuals are calculated relative to a third-order polynomial for ν , $\dot{\nu}$, and $\ddot{\nu}$ using a similar procedure.

The results of the timing analysis for the observed pulsars are given in Table 2. The columns list, respectively, the pulsar’s B1950 name, the rotation frequency, ν , the first frequency derivative, $\dot{\nu}$, and the second frequency derivative, $\ddot{\nu}$. The next four columns give the epoch of the ν measurement, the MJD range of the observations, the unweighted rms value remaining after a second-order fit σ_2 , and the unweighted rms value remaining after a third-order fit σ_3 .

3. Results

3.1. The Timing Behavior of 27 Pulsars on Long Time Scales

Lyne et al. (2010) found that changes in pulse shape parameters are correlated with changes in the spin-down parameters of some pulsars. At the PRAO, the pulsar signals are

received with a linearly polarized meridian telescope. For the majority of pulsars from our sample, the observed shape of the mean pulse profile varies from day to day because of either the influence of the Faraday effect or the lack of a sufficient number of individual pulses for an observing session. Under such conditions, we cannot determine our pulse shape changes and repeat a similar analysis of the pulse shape parameters and the spin-down parameters. Therefore, the pulse shape changes are not discussed in the later sections.

The timing behavior of the studied pulsars is shown in Figures 2(a)–(h). The residual plots for each pulsar are shown in two panels. The timing residuals relative to a simple $\nu, \dot{\nu}$ spin-down model are shown in the left-hand panels. The corresponding frequency residuals $\Delta\nu$ are shown in the right-hand panels. These plots are arranged in order of increasing characteristic age of the pulsars, $\tau_c = P/2\dot{P}$. The pulsar’s B1950 name and the pulse period (seconds) are indicated in each left-hand panel. The pulsar age in years is indicated on a logarithmic scale in each right-hand panel. The periods of the studied pulsars are between 0.1 and 3 s.

It is clearly seen in Figure 2 that the timing behavior of most pulsars in our sample significantly deviates from a simple $\nu, \dot{\nu}$ spin-down model. Such deviations, known as timing noise, may be a result of significant irregularities in the rotation rate of the pulsars. Table 2 shows that the timing residuals for all the observed pulsars are characterized by significant second derivatives that are too large to be attributed to pulsar spin-down. These values of $\ddot{\nu}$ testify that all our pulsars have a high level of timing noise.

Detailed inspection of the timing residuals plotted in Figure 2 shows that there is an appreciable correlation between the amplitude of the residual curve and the characteristic age of the pulsar—the smaller the amplitude of the residual curve, the older the pulsar. As seen in Figure 2(a), the timing residuals for younger pulsars have complex structures including cubic polynomial components with large amplitudes. As the age of a pulsar increases, we more often observe residuals that exhibit a quasi-periodic structure with smaller amplitudes, as is shown in Figure 2(c) for PSR B1642–03 and B1133+16, for example. The older pulsars mainly have the structures where noise-like variations dominate, as in Figure 2(g), for example, for the pulsars B0320+39 and B0809+74.

In order to study the effect of timing noise on the $\ddot{\nu}$ measurements, we analyze the timing residuals together with the frequency residuals and try to determine the causes of the large values of the measured $\ddot{\nu}$ for each given pulsar. We distributed all the observed pulsars into four groups according to the signatures of their timing residuals. The first group includes eight pulsars, in which the timing residuals take the form of a cubic polynomial. Five of these pulsars have experienced glitches in the past according to the literature. These pulsars have the largest $\ddot{\nu}$ values, as shown in Table 2. The second group includes seven pulsars that show

quasi-periodic variations in their timing residuals. The third group includes 10 pulsars that exhibit timing residuals where noise-like variations dominate. The fourth and final group is unique. This group includes two pulsars, B0823+26 and B1929+10, whose timing behavior demonstrates a rare phenomenon—a change in the sign of the second derivative $\ddot{\nu}$. Studying this phenomenon will help us to understand why pulsars with characteristic ages greater than $\tau_c > 10^5$ ys have both positive and negative $\ddot{\nu}$ values.

3.1.1. *The $\ddot{\nu}$ Values and Cubic Components in the Timing Residuals*

The first group includes eight pulsars that show cubic components in their timing residuals. The amplitude of the timing residuals for these pulsars varies from one quarter up to more than one pulse period over spans ranging from 19 to 34 yr. The characteristic ages of these pulsars range from 2×10^5 to 9×10^6 yr.

(1) **B1822–09.**

Shabanova (1998) was the first to detect slow glitches in the rotation frequency of the pulsar B1822–09. Slow glitches represent a unique glitch phenomenon that results in regular oscillations in the rotation frequency. A full pattern of the timing and frequency residuals for the pulsar B1822–09 over the 26 yr span between 1985 and 2012 is shown in Figures 2(a) and 2(b), respectively. These plots show that the pulsar experienced three discrete glitches (marked by the three arrows in the left-hand plot) and suffered a sequence of five slow glitches that occurred over the 1995–2004 interval. An oscillatory character of the timing and frequency residuals seen in both the plots over the interval 1995–2004 is due to the presence of slow glitches. The signature of the large discrete glitch that occurred in 2007 January (Shabanova 2009a) is clearly visible on the right side of the $\Delta\nu$ plot.

The difference between the signature of a slow glitch and that of a discrete glitch is clearly seen in Figure 6, where the time behavior of the frequency derivative $\dot{\nu}$ and the $\Delta\nu$ residuals are presented relative to the timing model 1991–1994 throughout the whole time span from 1985 to 2012. Here, the epochs of the three discrete glitches of 1994, 2006, and 2007 are marked by arrows pointing upward and the epochs at which the slow glitches occurred are marked by arrows pointing downward. It is seen in Figure 6(b) that while the discrete glitch of 2007 represents a sudden jump in the $\Delta\nu$ residuals, the slow glitches exhibit gradual exponential increases in the rotation frequency with a time scale of 200–300 days. Figure 6(a) displays the time behavior of $\dot{\nu}$, which has some surprising features. First, a gradual increase in $\Delta\nu$ is accompanied by a rapid decrease in the magnitude of $\dot{\nu}$ by $\sim 1\%$ – 2% of the initial value and a subsequent exponential increase back to its initial value.

Second, the peaks of $\Delta\dot{\nu}$, which characterize the steepness of the front in the residuals $\Delta\nu$, lie on a parabolic curve that is the envelope of these peaks. The existence of the envelope indicates that all of the slow glitches are components of one process that acted during the 10 yr between 1995 and 2004. The glitch history of PSR B1822–09 was described in detail in a series of papers (Shabanova 1998, 2005, 2007, 2009a; Shabanova & Urama 2000). The glitch parameters of this pulsar from the PRAO measurements are given in Table 3.

The final part of the oscillatory process over the interval 2000 January–2003 November in PSR B1822–09 was also observed by Zou et al. (2004). The authors have independently detected a glitch event with an unusual signature that occurred over this interval and have interpreted this glitch in terms of a slow glitch, as suggested by Shabanova (1998). In a sequence of five slow glitches, shown in Figure 6, this glitch is designated as the third one. The fourth glitch is very small and its signature is not seen. The glitch events in this pulsar were studied in a number of other papers (Hobbs et al. 2010; Yuan et al. 2010; Espinoza et al. 2011; Yu et al. 2013). Examining these papers shows that the glitch epochs, indicated in our Table 3, are generally in reasonable agreement with the measurements of other authors, but the interpretations of the glitch events are different. According to Table 1 of Espinoza et al. (2011), PSR B1822–09 has experienced six glitches between MJD 49940 and 54115 and none of these glitches was interpreted as a slow glitch. We cannot compare a full pattern of the PRAO glitch residuals, presented in Figure 6(b), with that of the JBO glitch residuals because Figures 6 and 7 of Espinoza et al. (2011) show separate residual plots for four different glitches. The idea of slow glitches has recently received support. Yu et al. (2013) suggested that the slow glitch-like events that result in the quasi-sinusoidal features in the timing residuals should be labelled as slow glitches.

Figure 7 displays the timing residuals for PSR B1822–09 after the glitch of 2007 relative to a simple spin-down model. The observed cubic term points to a large positive value $\ddot{\nu} = 14.4 \times 10^{-25} \text{ s}^{-3}$ that can be explained by the recovery from the discrete glitch. We conclude that rotational irregularities, such as slow glitches and discrete glitches, are the cause of the deviation of the timing behavior of this pulsar from a simple $\nu, \dot{\nu}$ spin-down model.

(2) B0919+06. As reported by Shabanova (2010), the slow glitch phenomenon was also detected in the rotation frequency of the pulsar B0919+06. Figure 2(a) shows the timing residuals relative to a timing model of $\nu, \dot{\nu}$, and $\ddot{\nu}$. It is seen that the residual curve displays a large quartic term with the amplitude approximately equal to half the pulsar period. Rapid oscillations that are imposed on this curve are interpreted as a sequence of slow glitches. The arrow in Figure 2(a) marks the epoch of a large glitch of magnitude $\Delta\nu/\nu \sim 1.3 \times 10^{-6}$ that occurred in 2009 November 5 (MJD 55140; Shabanova (2010)). The cubic component

of this complex structure corresponds to a large value $\ddot{\nu} \sim 2 \times 10^{-25} \text{ s}^{-3}$ which leads to a large braking index, $n \sim 80$.

A sawtooth-like character of the frequency residuals $\Delta\nu$, shown in Figure 2(b), implies that the rotation frequency of this pulsar underwent rapid oscillations with a time scale of about 600 days during the whole 30 yr period of observations. As discussed by Shabanova (2010), the cause of these oscillations lies in the continuous generation of similar slow glitches. These glitches are characterized by small absolute amplitudes of $3.5 \times 10^{-9} \text{ Hz}$, long rise times of 200 days, and relaxation time intervals of 400 days. The sequence of the observed slow glitches is well approximated by a periodic sawtooth-like function with a period of 600 days. Further observations of this pulsar are needed to study the relation between the discrete glitch and a process that continuously generates rapid oscillations identified with slow glitches. We conclude that rotational irregularities, such as long-term quasi-periodic oscillations and a sequence of slow glitches and a large discrete glitch, are responsible for the large measured $\ddot{\nu}$ values in this pulsar.

(3) B0355+54. Figure 2(a) displays the timing residuals obtained for the pulsar B0355+54 at the PRAO during the two observational intervals 1982–1986 and 1991–2012. This pulsar underwent two glitches in the 1980s. As reported by Lyne (1987), the first glitch occurred in 1985 (MJD 46077) and was quite small with $\Delta\nu/\nu \sim 6 \times 10^{-9}$. The second occurred in 1986 (MJD 46497) and was a giant glitch with $\Delta\nu/\nu \sim 4.4 \times 10^{-6}$. These glitches were also registered in the PRAO observations (Shabanova 1990). The glitch epochs are marked by two arrows in Figure 2(a).

Figure 2(a) shows that the timing residuals for PSR B0355+54 over the post-glitch interval 1991–2012 take the form of a cubic polynomial and are characterized by a significant $\ddot{\nu}$ value. The plotted cubic trend presents the residuals calculated relative to a simple $\nu, \dot{\nu}$ timing model 1991–2010 because all of the pulse arrival times gathered over the entire 1991–2012 interval cannot be described by a simple spin-down model within half the pulse period because of the presence of a large $\ddot{\nu}$. This plot shows that the amplitude of the cubic structure, equal to $\sim 125 \text{ ms}$, exceeds half the pulse period. The observed cubic trend corresponds to a positive value $\ddot{\nu} \sim 1.7 \times 10^{-25} \text{ s}^{-3}$ that gives a braking index of ~ 33 . It is evident that the observed cubic structure in the timing residuals is caused by the recovery from the 1986 glitch.

The corresponding frequency residuals presented in Figure 2(b) also indicate the presence of a large $\ddot{\nu}$. From this plot, it is seen that all the $\Delta\nu$ points lie on a parabolic curve that is due to the presence of a large $\ddot{\nu}$. Janssen & Stappers (2006) studied the timing behavior of this pulsar during $\sim 6 \text{ yr}$ between 1999 and 2005 and found four micro-glitches with sizes of $\Delta\nu/\nu \sim 0.4, 0.3, 0.4, \text{ and } 1.0 \times 10^{-10}$, respectively. The epochs of these events are marked by

vertical lines in Figure 2(b). It is seen that these small glitch events are consistent with the level of fluctuations in the $\Delta\nu$ curve. Therefore, they do not influence large-scale structure in the frequency residuals and they do not contribute to the measured value of $\ddot{\nu}$. We cannot compare our results with the JBO measurements because PSR B0355+54 is not included in the JBO sample (Hobbs et al. 2010).

The timing and frequency residuals for PSR B0355+54 after a fit of a third-order polynomial for ν , $\dot{\nu}$, and $\ddot{\nu}$ are presented in Figure 8. It is seen that the amplitude of the remaining residuals has considerably decreased. The $\Delta\nu$ curve is straightened. This plot, as well as Figure 2(b), shows that four micro-glitches, whose epochs are marked by the vertical lines, are local events and do not influence the measured value of $\ddot{\nu}$. In Figure 8, it is evident that the second derivative $\ddot{\nu}$ dominates the timing and frequency residuals over the whole span of observations of this pulsar. Thus, a large cubic trend visible in the timing residuals of PSR B0355+54 is caused by the recovery from the 1986 glitch.

(4) B2224+65. The timing residuals of PSR B2224+65 over the interval 1982–2012 are presented in Figure 2(a). This pulsar suffered a large glitch with a magnitude of $\Delta\nu/\nu \sim 1.7 \times 10^{-6}$ in 1976 (Backus et al. 1982). The glitch epoch is marked by an arrow in this plot. The plot shows that the timing residuals have a complex structure with a large amplitude of about 270 ms. The cubic component of this structure is characterized by a positive $\ddot{\nu}$, equal to $\sim 3 \times 10^{-26} \text{ s}^{-3}$, that leads to a braking index of 106. The corresponding frequency residuals $\Delta\nu$ are presented in Figure 2(b). We pay specific attention to an arc-like extended detail clearly seen in the $\Delta\nu$ curve between 1999 and 2007 (\sim MJD 51200–54100). Four vertical lines plotted on the $\Delta\nu$ panel mark the epochs of three micro-glitches with magnitudes of $\Delta\nu/\nu \sim 1.4, 0.8,$ and 1.9×10^{-10} , respectively, reported by Janssen & Stappers (2006), and the epoch of a fourth glitch with $\Delta\nu/\nu \sim 3.6 \times 10^{-10}$, reported by Yuan et al. (2010). The plot shows that all of these lines are in the range of the arc-like extended detail. Most likely, these small glitches are a consequence of a complex structure of the $\Delta\nu$ curve.

The pulsar B2224+65 is associated with the Guitar Nebula and is the fastest known pulsar. It has a large transverse velocity of 800–1600 km s^{-1} for a distance of 1–2 kpc. The motion of PSR B2224+65 through a medium with significant density fluctuations can cause changes in the DM that can be measured in timing observations (Chatterjee & Cordes 2004). We suppose that the arc-like extended detail in $\Delta\nu$ can be an important indication of the existence of DM variations for the pulsar B2224+65.

There are a number of arguments in favor of the DM variations. First, there is a discrepancy among the DM values measured by different authors at different epochs. As follows from Table 4, the difference among the measured DM values significantly exceeds the estimated measurement uncertainties. At the PRAO, the DM value was measured using

the phase shift between the two sets of the timing residuals obtained at the two observing frequencies of 102.746 (until 1998 May) and 111.646 MHz (after 1998 November). The timing residuals for PSR 2224+65, plotted in Figure 2(a), were calculated for the value $DM=36.226(5)$ pc cm⁻³. Secondly, the JBO residuals, plotted in Figure 3 of Hobbs et al. (2010), show a flatter structure compared with that of the PRAO residuals, plotted in Figure 2(a). The low-frequency timing measurements are very sensitive to changes in the DM. For example, a continuous increase in the DM by $\Delta DM \sim 0.2$ pc cm⁻³ during several years of observations will cause delay in the pulse arrival times registered at 112 MHz during this interval, where the delays can be as large as 66 ms. It accordingly follows that changes of the DM changes with time, if they exist, will more considerably influence the form of the residuals obtained at lower frequencies, for example, 112 MHz. Besides, as is shown in Figure 8, where the timing and frequency residuals are presented after a fit of a third-order polynomial, a remnant structure of the arc-like extended detail has the same shape, as in Figures 2(a) and 2(b). This result means that the $\Delta\nu$ variations over the interval 1999–2007 cannot be attributed to the presence of $\ddot{\nu}$. Reliable information about the DM variations can be obtained from a comparison of the high- and low-frequency timing data collected over the period 1982–2012 in the quasi-simultaneous observations of this pulsar at different observatories.

Figure 8 also shows that the micro-glitches, whose epochs are marked by the vertical lines in the $\Delta\nu$ plot, do not influence the large-scale structure of the frequency residuals. As in the case of PSR B0355+54, small glitch events are local events and do not contribute to the long-term behavior of $\ddot{\nu}$. We conclude that a large positive value of $\ddot{\nu}$ measured for the pulsar B2224+65 may be explained by the recovery from a large glitch in 1976. It is also very likely that the DM variations additionally contribute to the measured $\ddot{\nu}$ value.

(5) B1508+55. The pulsar B1508+55 experienced a small glitch of $\Delta\nu/\nu \sim 2.2 \times 10^{-10}$ that occurred in early 1973 (Manchester & Taylor 1974). Figure 2(a) displays the timing residuals for 18 yr of observations after 1993. The epoch of the 1973 glitch is marked by an arrow. The plotted timing residuals take the form of a cubic polynomial that is characterized by the negative value $\ddot{\nu} = -3.5 \times 10^{-26}$ s⁻³; this result leads to a braking index of -562. Figure 2(b) shows the time behavior of the frequency residuals $\Delta\nu$. From this plot, it is seen that all the $\Delta\nu$ points are well described by a parabolic curve despite noticeable quasi-sinusoidal deviations of these points from the approximating curve. A parabolic pattern of the $\Delta\nu$ changes means that the second derivative $\ddot{\nu}$ dominates the timing residuals during the entire observational interval. A quasi-sinusoidal structure in the rotation rate is clearly visible in Figure 8, where the timing and frequency residuals are shown after the removal of a cubic polynomial. It is seen that the post-fit timing residuals show two cycles of a quasi-periodic structure with a variable amplitude of about 30–10 ms. The corresponding

$\Delta\nu$ residuals also exhibit noticeable quasi-periodic variations in the rotation frequency.

Comparing with the results of Hobbs et al. (2010) shows that the signature of the timing residuals, presented in our Figure 2(a), is unlike that of the residuals, shown in their Figure 3. According to Table 1 of Hobbs et al. (2010), this pulsar was observed at the JBO over the 1982–2006 interval. At the PRAO, B1508+55 was observed at another interval, between 1993 and 2012. As is shown in Figure 5 of Hobbs et al. (2010), the timing residuals obtained from different section of the entire data span can have a different form. It is very likely that we observe this effect for this pulsar.

Thus, we found that the timing residuals of PSR B1508+55 are characterized by a large negative $\ddot{\nu}$. Its origin is uncertain. It is unlikely that the complex structure seen in the residuals of this pulsar can be a consequence of a small discrete glitch of 1973.

(6) B2020+28. The pulsar B2020+28 is not known to have glitched in the past. Nevertheless, the timing residuals seen in this pulsar have the form of a cubic polynomial corresponding to a positive $\ddot{\nu}$. Figures 2(a) and (b) exhibit the timing and frequency residuals that characterize the rotation of the pulsar over the 21 yr span from 1991 to 2012. The observed quasi-cubic trend in the timing residuals corresponds to a large value $\ddot{\nu} \sim 3 \times 10^{-26} \text{ s}^{-3}$, which gives a braking index $n \sim 330$. Figure 2(b) clearly displays that the changes in the $\Delta\nu$ residuals with time are well approximated by a parabolic curve that indicates the dominant character of $\ddot{\nu}$ in the rotation rate of the pulsar.

The timing and frequency residuals after subtraction of a cubic polynomial from the pulse arrival times are shown in Figure 8. We see that the remaining timing residuals have cyclical variations with small amplitude of ~ 8 ms. The corresponding $\Delta\nu$ residuals, plotted on the right panel, show noticeable quasi-periodic variations that range between $\pm 0.7 \times 10^{-9}$ Hz. We cannot compare our results with the JBO measurements because PSR B2020+28 is not included in the JBO sample (Hobbs et al. 2010).

We hypothesize that the cubic form of the timing residuals corresponding to a large positive derivative $\ddot{\nu}$ could be the consequence of an unobserved glitch event that occurred in B2020+28 before our observations began in 1991.

(7) B0943+10. Figure 2(c) shows the timing residuals for the pulsar B0943+10 over the 30 yr span from 1982 to 2012. We see that the timing residuals are characterized by a large cubic trend corresponding to a negative $\ddot{\nu}$. The plotted residuals are presented relative to the timing model 1982–2008, as not all the pulse arrival times can be described by a simple spin-down model within half the pulsar period because of the presence of a large $\ddot{\nu}$. This plot shows that the deviations from the simple timing model are very large, about ~ 1500 ms, and that they are more than one pulse period. The cubic trend in the timing residuals

corresponds to a negative value $\ddot{\nu} \sim -7 \times 10^{-26} \text{ s}^{-3}$. This value yields a braking index $n \sim -7924$. The frequency residuals, presented in Figure 2(d), show a parabolic change of the $\Delta\nu$ points with time. This plot confirms that a large $\ddot{\nu}$ dominates the timing residuals of this pulsar over the whole observational interval.

The timing residuals after the removal of a cubic term are shown in the left panel of Figure 8. A large quartic term visible in the remaining timing residuals points to the presence of a third significant frequency derivative. The corresponding frequency residuals $\Delta\nu$ are plotted in the right panel of Figure 8. The noticeable downward slope of the $\Delta\nu$ curve also indicates the presence of a third frequency derivative.

Comparing our timing residuals, shown in Figures 2 and 8, and the JBO timing residuals, shown in Figure 3 and 13 of Hobbs et al. (2010), reveals a discrepancy between the signatures of these residual curves. The reason for this discrepancy is related to the presence of the third derivative in the rotation rate of this pulsar and the different length of the data sets analyzed. The JBO data set covers the interval 1983–2006 (Table 1 of Hobbs et al. (2010)); the PRAO data set spans more time and covers the interval 1982–2012. The influence of the third derivative becomes noticeable after 2006, as is seen in Figure 2(c). If we analyze the timing data over the same interval 1983–2006, then the discrepancy between the PRAO and JBO residuals disappears.

Thus, we found that the timing residuals for PSR B0943+10 have the form of a cubic polynomial corresponding to a significant negative second derivative $\ddot{\nu}$. Most likely, the pulsar B0943+10 could have had glitches in its rotation frequency in the past. Then, a large value of $\ddot{\nu}$ could be the consequence of these glitch events that occurred prior to our observations. However, the reason for the negative sign of $\ddot{\nu}$ is unclear.

(8) B1737+17. In the literature, there are no indications that the pulsar B1737+17 glitched in the past, but Figure 2(e) shows a clear cubic trend in the timing residuals that can be considered the signs of a recovery from a glitch. The plotted timing residuals are presented over the interval 1978–2012. The first point from the JPL data set belongs to 1978 December. It is possible that this pulsar suffered a glitch before the JPL timing observations started. The cubic term in the timing residuals corresponds to a positive value $\ddot{\nu} \sim 2 \times 10^{-26} \text{ s}^{-3}$. This value gives a braking index of ~ 5181 . The frequency residuals presented in Figure 2(f) show that all the $\Delta\nu$ points lie on a parabolic curve. This result means that a large $\ddot{\nu}$ dominates the rotation behavior of this pulsar over the entire interval of the observations. The timing and frequency residuals after the removal of a cubic term are given in Figure 8. The remaining residuals show a noticeable long-term quasi-periodic structure. Comparison with the results of Hobbs et al. (2010) shows that the timing residuals, presented in our Figures 2(e) and 8, are in good agreement with the residuals given in their Figures 3 and

13.

We may suppose that a large positive $\ddot{\nu}$ measured in the pulsar B1737+13 could be caused by the recovery from an unobserved glitch that occurred prior to 1978, before the JPL observations had begun.

Summary. We found that all eight pulsars whose timing residuals take the form of a cubic polynomial have large second frequency derivatives that range between $\ddot{\nu} \sim (0.2 - -20) \times 10^{-25} \text{ s}^{-3}$. The long-term structure of these timing residuals is determined by such rotational irregularities as discrete glitches, slow glitches, and quasi-periodic oscillations.

3.1.2. *The $\ddot{\nu}$ Values and Cyclical Signatures in the Timing Residuals*

The second group includes seven pulsars that show cyclical or quasi-periodic signatures in their timing residuals. The maximum amplitude of the cyclical changes in the timing residuals for the different pulsars varies from 4% to 40% of their period over the 30–44 yr spans of the observations. The characteristic ages of these pulsars range from 3×10^6 to 6×10^7 yr.

(1). B2217+47. Figure 2(c) shows the timing residuals for PSR B2217+47 over the 42 yr time span between 1970 and 2012. From this plot, we see that the timing residuals have a quasi-periodic structure over the interval 1970 January–2011 October. This structure is characterized by maxima spacing between cycles of about 10–14 yr and an amplitude of about 5–10 ms. We detected that this pulsar experienced a small glitch that occurred in 2011 October 24 (MJD 55858). The glitch epoch is marked by an arrow. The $\Delta\nu$ residuals, plotted in Figure 2(d), show that the glitch has a small absolute amplitude of $\Delta\nu \sim 2.3 \times 10^{-9}$ Hz. This value corresponds to a fractional increase in the rotation frequency of $\Delta\nu/\nu \sim 1.3 \times 10^{-9}$. The glitch parameters are given in Table 5. The value of the second derivative measured before the glitch occurred is $\ddot{\nu} \sim -7 \times 10^{-28} \text{ s}^{-3}$, which gives a braking index $n \sim -14$.

Figure 9 shows the timing and frequency residuals after the removal of the cubic trend over the interval before the glitch occurred. The quasi-periodic structure of the post-fit residuals is clearly seen in these plots. The $\Delta\nu$ curve changes within a range of $\Delta\nu \pm 0.8 \times 10^{-9}$ Hz. Comparison with the results of Hobbs et al. (2010) shows that our residuals, plotted in Figure 2(c) before the glitch occurred, are in good agreement with their timing residuals, given in their Figure 3.

We conclude that the measured negative value of $\ddot{\nu}$ is associated with the long-term quasi-periodic variation observed in the timing residuals for PSR B2217+47 over the interval

1970–2011.

(2). **B1642–03.** Shabanova (2009b) reported the detection of slow glitches in the rotation rate of the pulsar B1642–03 and showed that the observed pattern of cyclical timing residuals is a result of the continuous generation of slow glitches whose amplitudes are modulated by some periodic large-scale process. Slow glitches in this pulsar show striking properties that allow us to predict the epochs and the amplitudes of new glitches in the pulsar’s rotation rate. The cyclical character of the timing and frequency residuals for PSR 1642–03 is well seen in Figures 2(c) and 2(d), respectively, which present these residuals over the 43.5 yr time span from 1968 to 2012. With respect to the results of Shabanova (2009b), we extend the observational interval by including three years of new observations.

In Shabanova (2009b), we showed that the cause of the cyclical oscillations in the timing residuals of PSR B1642–03 is the continuous generation of slow glitches. These glitches are characterized by long rise times of about 500 days and exponential relaxation over several years after a glitch. The observed slow glitches have two surprising properties. First, the amplitude of these glitches and the time interval until the following glitch obey a strong linear relation—the larger the glitch amplitude, the larger the time interval to the next glitch. This property allows us to predict epochs of new glitches. Secondly, the amplitude of these glitches is modulated by a periodic large-scale sawtooth-like function. As a result of such modulation, the glitch amplitudes change discretely in a strictly certain sequence assigned by the sawtooth-like function. This property allows us to predict the amplitudes of new glitches.

In our previous paper (Shabanova 2009b), we analyzed the properties of eight slow glitches. According to the predictions of that paper, the ninth glitch will occur in ~ 2013 . Figures 2(c) and (d) show that this prediction has come true. The maximum of the ninth glitch is clearly seen in the timing residuals, plotted in Figure 2(c). The maximum of the $\Delta\nu$ residuals, plotted in Figure 2(d), occurs around MJD 56100. The observed epoch is slightly earlier than the predicted epoch of MJD 56300. Nevertheless, these epochs are in agreement within the time resolution of ~ 300 days. Further observations are needed to determine the amplitude of the ninth glitch. We should measure the relaxation time interval after the ninth glitch. According to Table 2 of Shabanova (2009b), for the 43 yr modulation scheme including eight glitches, this information will be obtained at the end of 2013 or in the beginning of 2014. In this case, the observed amplitude of the ninth glitch should be equal to $\Delta\nu_g \sim 2.4 \times 10^{-9}$ Hz. In the case of the two other modulation schemes with modulation periods of 53 yr and 60 yr, the relaxation time interval will be known in the middle of 2015. Then, the observed amplitude of the ninth glitch should be equal to $\Delta\nu_g \sim 3.9 \times 10^{-9}$ Hz. These two schemes will differ starting with the 10th glitch that should occur in ~ 2018 .

The cyclical structure in this pulsar is characterized by a positive value $\ddot{\nu} \sim 1.3 \times 10^{-27} \text{ s}^{-3}$ that yields a braking index $n \sim 23$. We suppose that the large measured value of $\ddot{\nu}$ in PSR B1642–03 is caused by the continuous generation of slow glitches over the entire period of observations 1968–2012.

Another point of view was presented by Lyne et al. (2010), who suggested that the observed oscillations in PSR B1642–03 can be accounted for by magnetospheric regulated dual-state switching. In Figure 2(c), it is seen that the predictability of the cycles in oscillatory behavior of this pulsar testify that the interpretation of this process by slow glitch events is preferable.

(3). B1133+16. The bottom panel of Figure 2(c) presents the timing residuals for the pulsar B1133+16 over the time span of 43 yr between 1969 and 2012. We see that the timing residuals have a quasi-periodic character with an amplitude of ~ 40 ms and maxima spacing of ~ 28 yr. These residuals are characterized by a positive value $\ddot{\nu} \sim 1 \times 10^{-27} \text{ s}^{-3}$ that gives a braking index $n \sim 131$. The corresponding frequency residuals $\Delta\nu$, presented in Figure 2(d), have a similar quasi-periodic structure. The rotation frequency changes within a range $\Delta\nu$ of $\pm 0.4 \times 10^{-9}$ Hz. The observed quasi-periodic pattern of the timing residuals is in good agreement with that of the timing residuals, given in Figure 3 of Hobbs et al. (2010).

The timing and frequency residuals of PSR B1133+16 after the subtraction of the polynomial for ν , $\dot{\nu}$ and $\ddot{\nu}$ maintain a quasi-periodic structure, as is seen in Figure 9. Thus, an appreciable $\ddot{\nu}$ value, measured for PSR B1133+16, is associated with the long-term quasi-periodic variation observed in the timing residuals of this pulsar.

(4) B0329+54. The timing residuals of PSR B0329+54 are shown in Figure 2(e) over the 43.5 yr time span from 1968 to 2012. We see that the first half of the timing residuals exhibit a long-term quasi-periodic variation that is superimposed on a cubic trend with a rather large amplitude. The parabolic character of the $\Delta\nu$ residuals, which are plotted in Figure 2(f), also testifies that a significant $\ddot{\nu}$ dominates in the pulsar rotation rate over the entire interval of observations, despite a noticeable quasi-sinusoidal structure visible in the first part of the $\Delta\nu$ curve. The observed timing residuals are characterized by a positive value $\ddot{\nu} \sim 3 \times 10^{-27} \text{ s}^{-3}$ that leads to a braking index of ~ 297 .

Demianski & Proszynski (1979) were the first to argue for the presence of a planet around the pulsar B0329+54. The authors reported the existence of a quasi-sinusoidal modulation with a period of 3 yr in pulse arrival times and supposed that a small planet around the pulsar could cause such a modulation. The planetary interpretation was supported by Shabanova (1995), who reported the existence of a quasi-sinusoidal modulation with a pe-

riod of 16.9 yr in the timing residuals and showed that a 3 yr periodicity is clearly seen in the JPL data after removing the main 16.9 yr periodicity. Further observations by Konacki et al. (1999) showed that there is no evidence for the presence of two planet-mass bodies on the 3 yr and 16.9 yr orbits around this pulsar. The authors concluded that the observed quasi-periodicity in the timing residuals of this pulsar may be attributed to the variations in the rotation frequency or free precession of a neutron star. According to Hobbs et al. (2010), the JBO data set shows no evidence for either a 3 yr or a 16.9 yr periodicity and therefore there is no evidence for a planetary companions to this pulsar.

We agree with this conclusion of Hobbs et al. (2010). In Figure 9, which shows the residuals for PSR B0329+54 after the removal of a cubic term from the arrival times, we see that a 16.9 yr periodicity existed over the interval 1968–1995 and is not repeated in further observations after 1995. Note that similar periodicities can be observed in the rotation frequency of other pulsars. For example, Figure 10 shows the timing residuals for two pulsars, B0823+26 and B1541+09, which contain two cycles of a quasi-periodic structure. In the case of B1541+09, the two cycles of the oscillatory residual curve are well described by a sinusoidal function with a period of ~ 7 yr. The observed quasi-periodic structure is not repeated in further observations. This example illustrates how a quasi-sinusoidal structure in the timing residuals can confuse the observer if the observational interval of the given pulsar is not sufficiently long.

It is very likely that the cubic trend seen in the timing residuals of Figure 2(e) and the parabolic character of the corresponding $\Delta\nu$ residuals, presented in Figure 2(f), both are the result of a large glitch that took place in the distant past. In this case, the measured $\ddot{\nu}$ value in the pulsar B0329+54 can be an echo of that previous event. In Figure 2(f), we see that the presence of cyclical variation in the rotation rate influences the pulsar timing behavior only on rather short intervals. We conclude that the large $\ddot{\nu}$ value of this pulsar is due to the presence of long-term cyclical variations and probably the influence of an odd glitch event.

(5) B0950+08. Figure 2(e) shows the timing residuals for the pulsar B0950+08 over the 43.5 yr time span from 1968 to 2012. The plotted timing residuals demonstrate a structure varying with time. This structure is characterized by a negative value $\ddot{\nu} \sim -6 \times 10^{-27} \text{ s}^{-3}$ that gives a braking index $n \sim -1979$. The $\Delta\nu$ residuals, plotted in Figure 2(f), also indicate some changes in the rotation frequency ranging from 0 to $-3 \times 10^{-9} \text{ Hz}$. The removal of a cubic term from the arrival times reduces the amplitude of the timing residuals, as is shown in Figure 9. Thus, we suppose that a long-term cyclical structure is the cause of the significant $\ddot{\nu}$ measured in the timing residuals of this pulsar.

(6) B1541+09. The timing and frequency residuals for PSR B1541+09 are given in Figures 2(g) and (h), respectively, over the 30 yr interval from 1982–2012. The timing

residual plot shows a cyclical structure that changes its amplitude and period with time. A quasi-periodic oscillation seen over the interval 1997–2010 was shown on a large scale before, in Figure 10. This plot shows that the two cycles of the observed quasi-periodic structure are well described by a sinusoidal function with a period of ~ 7 yr and an amplitude of 10 ms. This periodic structure is not repeated in further observations, as follows from Figure 2(g). The frequency residuals, plotted on the right panel, also exhibit the presence of cyclical changes in $\Delta\nu$ that are within the range of $\pm 1 \times 10^{-9}$ Hz. The observed timing residuals are characterized by a positive value $\ddot{\nu} \sim 9 \times 10^{-28} \text{ s}^{-3}$ that gives a braking index ~ 2012 .

Figure 9 shows that the timing and frequency residuals maintain a cyclical structure after the removal of a cubic term from the arrival times. Comparison with the results of Hobbs et al. (2010) shows that the signature of the PRAO timing residuals is generally in reasonable agreement with that of the JBO residuals, plotted in their Figure 3 up to 2006. One cycle of the quasi-sinusoidal periodicity examined above is present at the very end of the JBO data span. It is evident that the presence of cyclical changes in the rotation frequency is the cause of the appreciable value of $\ddot{\nu}$ in PSR B1541+09. The resemblance of the timing residuals to the quasi-sinusoidal structure with a period of ~ 7 yr is an interesting feature of the residuals. This result requires further research on the rotation frequency of this pulsar.

(7) B2016+28. Figure 2(g) displays the timing residuals for PSR B2016+28 over the 43.5 yr time span between 1968 and 2012. In this plot, we see an appreciable cubic trend with an amplitude of about 30 ms. The parabolic character of the frequency residuals, presented in Figure 2(h), also indicates the dominant influence of a rather significant $\ddot{\nu}$ over the entire observational interval. The observed timing residuals are characterized by a positive value $\ddot{\nu} \sim 3 \times 10^{-27} \text{ s}^{-3}$ that gives a braking index $n \sim 21186$. In Figure 9 that shows the timing and frequency residuals after the removal of a cubic term from the arrival times, we see that the remaining residuals exhibit a long-term quasi-periodic structure. The signature of the timing residuals, presented in our Figure 2(g), is in agreement with that result, as shown in Figure 3 of Hobbs et al. (2010).

We suppose that the parabolic character of the $\Delta\nu$ curve for this pulsar, shown in Figure 2(h), can be a consequence of the recovery from an old discrete glitch. As in the case of PSR B0329+54, the deviation of the timing behavior of PSR B2016+28 from a simple $\nu, \dot{\nu}$ spin-down model can be explained by the presence of long-term quasi-periodic variations and probably the influence of a prior glitch event.

Summary. We found that all seven pulsars whose timing residuals show a quasi-periodic signature have measurable $\ddot{\nu}$ values that range between $\ddot{\nu} \sim (0.7 - -6) \times 10^{-27} \text{ s}^{-3}$. The structure seen in the timing residuals of these pulsars is determined by such rotational irregularities as small discrete glitches, slow glitches, long-term quasi-periodic processes, and

probably the influence of prior glitch events.

3.1.3. The $\ddot{\nu}$ Values and Noise-like Structure of the Timing Residuals

The third group includes 10 pulsars whose timing residuals have noise-like variations that dominate at a level of less than 1% of a pulse period over time spans from 21 to 34 yr. The characteristic ages of these pulsars are more than 3×10^6 yr.

(1) B0834+06. The top panel of Figure 2(c) displays the timing residuals for PSR B0834+06 over the 34 yr span between 1978 and 2012. This pulsar has a long period of 1.27 s and a sufficiently large period derivative 6.8×10^{-15} , indicating that it is a relatively young pulsar with $\tau_c \sim 3 \times 10^6$ yr. The study of its rotation showed that this pulsar has very stable timing behavior in which rms residuals are $\sim 300 \mu\text{s}$ over the entire time span. Figure 2(d) shows that weak variations in the $\Delta\nu$ residuals range between $\pm 0.1 \times 10^{-9}$ Hz. The timing residuals of this pulsar are characterized by a positive value $\ddot{\nu} \sim 1 \times 10^{-28} \text{ s}^{-3}$. This value yields a braking index $n \sim 4$ that is very close to the canonical braking index $n = 3$, expected from the simple magnetic dipole braking. It is very likely that the timing noise in this pulsar can be accounted for by magnetic dipole braking. In this case, a measurement of the deterministic $\ddot{\nu}$ value will be possible in the near future.

(2) B2110+27. Figure 2(e) exhibits the timing residuals for this pulsar over the 28 yr time span from 1984 to 2012. The observed residuals take the form of a cubic polynomial with a very small amplitude of ~ 4 ms. Figure 2(f) shows that variations in the $\Delta\nu$ residuals are rather small and range between $\pm 0.3 \times 10^{-9}$ Hz. The timing residuals are characterized by a positive value $\ddot{\nu} \sim 4 \times 10^{-28} \text{ s}^{-3}$ that yields a braking index $n \sim 108$. We see that the observed shape of the timing residuals resembles a damped cubic trend.

(3) B2303+30. Figure 2(e) displays the timing residuals for PSR B2303+30 over the 21 yr span between 1991 and 2012. A weak cubic trend is visible in these residuals. The observed variations in the $\Delta\nu$ residuals are within the range of $\pm 0.5 \times 10^{-9}$ Hz, as is shown in Figure 2(f). The timing residuals are characterized by a negative value $\ddot{\nu} \sim -9 \times 10^{-28} \text{ s}^{-3}$ that gives a braking index $n \sim -449$.

(4) B1919+21. The timing residuals for PSR B1919+21 are presented in Figure 2(e) over the 34 yr data span from 1978 to 2012. The pulsar shows a weak timing noise in which rms residuals are ~ 1 ms. The $\Delta\nu$ residuals, plotted in Figure 2(f), exhibit random variations that range between $\pm 0.2 \times 10^{-9}$ Hz. The observed timing residuals are characterized by a negative value $\ddot{\nu} \sim -5 \times 10^{-29} \text{ s}^{-3}$ that gives a braking index $n \sim -65$.

(5) **B1839+56**. The bottom panel of Figure 2(e) exhibits the timing residuals of PSR B1839+56 over the 29 yr data span from 1983 to 2012. The timing residuals take the form of a cubic polynomial with an appreciable amplitude of about 7 ms, which is still less than 0.5% of a pulse period. The corresponding changes in the $\Delta\nu$ residuals, plotted in Figure 2(f), are weak and are within a range $\Delta\nu$ of $\pm 0.3 \times 10^{-9}$ Hz. We may be observing the damped oscillations of a more long-term cyclical process. The timing residuals are characterized by a negative value $\ddot{\nu} \sim -6 \times 10^{-28} \text{ s}^{-3}$ that gives a braking index $n \sim -1152$.

(6) **B2315+21**. The top panel of Figure 2(g) shows the timing residuals for this pulsar over the 21 yr data span from 1991 to 2012. The timing residuals exhibit a noise-like structure. The corresponding changes in the $\Delta\nu$ residuals, presented in Figure 2(h), range between $\pm 0.4 \times 10^{-9}$ Hz. The timing residuals are characterized by a negative value $\ddot{\nu} \sim -2 \times 10^{-28} \text{ s}^{-3}$, that gives a braking index $n \sim -496$.

(7). **B0138+59**. The timing residuals for this pulsar are shown in Figure 2(g) over the 29 yr time span from 1983 to 2012. A noise-like structure is visible in the timing residuals. The variations of the $\Delta\nu$ residuals, plotted in Figure 2(h), are within a small range $\Delta\nu$ of $\pm 0.2 \times 10^{-9}$ Hz. The timing residuals are characterized by a positive value $\ddot{\nu} \sim 2 \times 10^{-29} \text{ s}^{-3}$ that gives a braking index $n \sim 215$.

(8) **B1821+05**. Figure 2(g) displays the timing residuals for PSR B1821+05 over the 21 yr time span between 1991 and 2012. The timing residuals show a noise-like structure. Figure 2(h) shows that the variations of the $\Delta\nu$ residuals are within a range of $\pm 0.4 \times 10^{-9}$ Hz. The timing residuals are characterized by a positive value $\ddot{\nu} \sim 2 \times 10^{-28} \text{ s}^{-3}$ that gives a braking index $n \sim 1825$.

(9) **B0320+39**. Figure 2(g) shows the timing residuals for this pulsar over the 32 yr time span from 1980 to 2012. Noise-like variations are visible in the timing residuals. The variations in the $\Delta\nu$ residuals range between $\pm 0.2 \times 10^{-9}$ Hz, as is shown in Figure 2(h). The timing residuals are characterized by a positive value $\ddot{\nu} \sim 2 \times 10^{-29} \text{ s}^{-3}$ that gives a braking index $n \sim 1455$.

(10). **B0809+74**. The bottom panel of Figure 2(g) displays the timing residuals for PSR B0809+74 over the 33 yr data span from 1979 to 2012. The oldest pulsar in our sample demonstrates timing residuals with a noise-like structure. Figure 2(h) shows that variations in the $\Delta\nu$ residuals range between $\pm 0.3 \times 10^{-9}$ Hz. The timing residuals are characterized by a positive value $\ddot{\nu} \sim 5 \times 10^{-29} \text{ s}^{-3}$. This value yields a braking index of 3717.

Figure 11 shows the timing residuals for the 10 pulsars after the removal of a cubic term from the pulse arrival times. We see that most pulsars in this group exhibit random variations in the remaining timing residuals.

Summary. We found that all 10 pulsars whose timing residuals are dominated by noise-like variations show $\ddot{\nu}$ values that range between $\ddot{\nu} \sim (2 - -10) \times 10^{-29} \text{ s}^{-3}$. The measured $\ddot{\nu}$ values are on the boundary of the precision of our measurements, which is estimated to be $\sim 1 \times 10^{-28} \text{ s}^{-3}$. We suppose that the observed $\ddot{\nu}$ values for these pulsars arise because of the limited precision of our measurements, which is due to short observing intervals. As discussed in Livingstone et al. (2005), hundreds of years of observations are required to measure $\ddot{\nu}$ due to deterministic spin-down law in the middle-aged pulsars.

3.2. Detection of a Change in the Sign of $\ddot{\nu}$ for Pulsars B0823+26 and B1929+10

The fourth group includes two pulsars whose timing residuals exhibit more complex structure compared with the previous groups. The main feature of the rotation of these pulsars is that their rotation parameters ν , $\dot{\nu}$, $\ddot{\nu}$ can undergo a rapid change. This change is accompanied by a change in the sign of the second frequency derivative $\ddot{\nu}$. As a consequence of this phenomenon, the rotation behavior of these pulsars cannot be described by one ν , $\dot{\nu}$, $\ddot{\nu}$ timing model within one pulse period over a long time span of tens of years. Glitch events have nothing to do with this situation. We show that two different timing models, each of which includes $\ddot{\nu}$ of an opposite sign, are required for the description of the rotation behavior of these pulsars over the 43 yr span of data analyzed. The characteristic age of PSR B0823+26 is $\sim 5 \times 10^6$ yr and that of B1929+10 is $\sim 3 \times 10^6$ yr.

3.2.1. Evidence for a Sudden Change in the Sign of $\ddot{\nu}$ for PSR B0823+26

Figure 2(c) displays the timing residuals for PSR B0823+26 over the 43 yr span from 1969 to 2012. The combined data set includes the JPL data between 1969 and 1983 and the PRAO data between 1981 and 2012. A detailed analysis of the data showed that all the pulse arrival times gathered over the 1969–2012 interval cannot be described by a simple ν , $\dot{\nu}$ model within a pulse period because of the presence of a large $\ddot{\nu}$. These arrival times also cannot be described within a pulse period by a timing model including the second derivative $\ddot{\nu}$. The cause of this situation is not connected with glitch events.

In order to demonstrate the complex character of the rotation behavior of this pulsar over the entire observational period 1969–2012, we plotted the timing residuals relative to a simple spin-down model 1981–1986, as is shown in Figure 2(c). From this plot, we see that the deviation of the residual curve with respect to a zero line comprises approximately 1700

ms, more than three pulse periods. In order to keep track of the pulsar rotation over a long time span, we eliminated the phase jump in the residual curve by adding one period when the curve deviated by more than one pulse period.

The cause of such a deviation becomes more clear if we consider the frequency residuals shown in Figure 2(d). Here, the $\Delta\nu$ residuals are presented relative to the same spin-down model 1981–1986. We see that the $\Delta\nu$ curve has a distinct break in 1974 November (MJD 42364). The break separates two regions with different rotation frequency behaviors and is a cross point of the two curves having convex and concave shapes. It is known that such curves are characterized by opposite signs of $\ddot{\nu}$. This property means that the break in the frequency residuals is accompanied by a change in the sign of the second frequency derivative $\ddot{\nu}$. Further analysis confirms that the sign of $\ddot{\nu}$ is reversed at this point. Our purpose is to show that: (1) the two timing models, including $\ddot{\nu}$ of the opposite signs, are required to describe the rotation behavior of PSR B0823+26 over the entire 1969–2012 interval, (2) the break in the $\Delta\nu$ curve causes a change in the sign of the second derivative $\ddot{\nu}$, and (3) the break in the $\Delta\nu$ curve causes a distinct jump in the first derivative $\dot{\nu}$.

Figure 12 shows a detailed picture of the timing behavior of the pulsar B0823+26. The top panel demonstrates how the entire data set for this pulsar can be described by two independent timing models, including $\ddot{\nu}$ with opposite signs. The first interval (**I**) indicates a maximum interspace from the first point, in which the data set can be described by one timing model of ν , $\dot{\nu}$, and $\ddot{\nu}$ within half a pulse period. This interval is 1969–1984 (MJD 40264–45873). The obtained timing residuals are marked by open circles. An increase of this interspace to the right at one following point from the data set already causes a phase jump of more than a pulse period.

The second interval (**II**) indicates a maximum interspace from the last point of the data set (the rightmost point on the X -axis) to the earlier point in the data set (the leftmost point on the X -axis), in which the data set can be well described by another timing model of ν , $\dot{\nu}$, and $\ddot{\nu}$ within half a pulse period. The indicated interval is 1971–2012 (MJD 41279–55973). The obtained timing residuals are marked by solid circles. An increase of this interspace to the left at one previous point from the data set already causes a phase jump of more than a pulse period. The measured rotation parameters for these timing models include second derivatives $\ddot{\nu}$ with opposite signs: $\ddot{\nu} = -5.51 \times 10^{-25} \text{ s}^{-3}$ over the 1969–1984 interval and $\ddot{\nu} = 0.55 \times 10^{-25} \text{ s}^{-3}$ over the 1971–2012 interval. So, we have showed that two timing models are required to describe the pulsar’s rotation behavior over the 1969–2012 interval and these models include $\ddot{\nu}$ of opposite signs.

The middle panel of Figure 12 shows how a change in the sign of $\ddot{\nu}$ has an effect on the rotation frequency of the pulsar. The vertical line marks the time of the break in the

frequency residuals which, according to Figure 2(d), took place in 1974 November (MJD 42364). The plotted frequency residuals $\Delta\nu$ are presented relative to the two ν , $\dot{\nu}$, $\ddot{\nu}$ timing models: 1969–1974 (before the break) and 1974–2012 (after the break). The mean rotation parameters for these timing models are given in Table 2, from which it can be seen that these models include second derivatives of $\dot{\nu}$ with opposite signs. At first, we present the $\Delta\nu$ residuals relative to the first timing model 1969–1974, including $\ddot{\nu} < 0$ (open circles). From this plot, we see that the $\Delta\nu$ residuals correspond well with the zero line in section A (before the break). Beyond section A, the $\Delta\nu$ curve sharply deviates with respect to the zero line. This result means that the values of ν calculated from the model 1969–1974 do not correspond to the actual rotation frequencies existing after the break. A similar picture is observed for the other model 1974–2012, including $\ddot{\nu} > 0$ (solid circles). In section B (after the break), the $\Delta\nu$ residuals correspond well with the zero line. Ahead of section B, the $\Delta\nu$ curve abruptly declines downwards with respect to the zero line.

Both of these plots, as well as Figure 2(d), show that the point of the break is formed as a result of a sudden change in the slope of the $\Delta\nu$ curve within the framework of the given model. The sharp turn in the $\Delta\nu$ curve is the cause of a change in the sign of the second derivative $\ddot{\nu}$. The break is a rapid event as it happens within ~ 300 days, which is the time resolution. So, we have shown that the break in the $\Delta\nu$ curve is accompanied by a change in the sign of the second frequency derivative $\ddot{\nu}$.

The bottom panel of Figure 12 shows the first frequency derivative $\dot{\nu}$ as a function of time. The time behavior of $\dot{\nu}$ is identical for all the timing models that were mentioned above. The observed changes in the $\dot{\nu}$ behavior are the effect of the changes in the $\Delta\nu$ curve. This statement is confirmed by a visual comparison of this $\dot{\nu}$ plot with the $\Delta\nu$ plot, presented in Figure 2(d). From the bottom panel of Figure 12, we see that the observed appearance of the $\dot{\nu}$ curve testifies to a change in the sign of $\ddot{\nu}$. The long-term behavior of the $\dot{\nu}$ curve can be described as a fast increase of $|\dot{\nu}|$ before the break (section A), a distinct jump in the magnitude of $\dot{\nu}$ at the point of the break, and the gradual decrease of $|\dot{\nu}|$ after the break (section B). The break in the $\Delta\nu$ curve produces a distinct jump in the first derivative $\dot{\nu}$. The magnitude of the jump in $\dot{\nu}$ equals $\Delta\dot{\nu} \approx 0.12 \times 10^{-15} \text{ s}^{-2}$. It makes up $\sim 2\%$ of the mean value of $\dot{\nu} \approx -6.07 \times 10^{-15} \text{ s}^{-2}$. So, we have shown that the break in the $\Delta\nu$ curve causes a jump in the first derivative $\dot{\nu}$.

It should be noted that the jump in $\dot{\nu}$ for the pulsar B0823+26 was known earlier. Gullahorn & Rankin (1982) detected an event in $\dot{\nu}$ in early 1975 (JD 2442500). This time agrees well with our time of the break in the $\Delta\nu$ curve (JD 2442364). According to their Figure 11, the size of the jump equals $\Delta\dot{\nu}/\dot{\nu} \sim 2 \times 10^{-2}$, which agrees well with our measurement of the jump in $\dot{\nu}$. Cordes & Downs (1985) also noticed that B0823+26 exhibits

a large discontinuity in both P and \dot{P} near JD 2442600. These events are clearly visible in their Figure 6. Later, the timing noise of PSR B0823+26 was analyzed by Baykal et al. (1999). The break in the frequency residuals of this pulsar is clearly seen in their Figure 1. The time of the break can be estimated from this plot to be \sim JD 2442400. This time agrees well with our result.

We pay attention to the short-term quasi-periodic variations seen in the timing behavior of PSR B0823+26 in all three panels of Figure 12. Two cycles of a quasi-periodic structure of the timing residuals over the interval 1991–2008 were shown before on a large scale in Figure 10. Short-term quasi-periodic variations in the behavior of $\dot{\nu}$, seen clearly in the bottom panel of Figure 12, are the cause of variations in the $\ddot{\nu}$ values measured during different time spans. This plot illustrates why the measured values of $\ddot{\nu}$ may be different at different parts of the data span analyzed, as was earlier remarked by Hobbs et al. (2004) (see their Figure 7). On the contrary, the long-term behavior of the second derivative $\ddot{\nu}$ is associated with a linear trend that is observed in the first derivative $\dot{\nu}$ over the entire 38 yr time span between 1974 and 2012.

3.2.2. Evidence for a Sudden Change in the Sign of $\ddot{\nu}$ for PSR B1929+10

The pulsar B1929+10 is the second pulsar in our research, after PSR B0823+26, for which the phenomenon of a change in the sign of the second derivative $\ddot{\nu}$ was revealed. Figure 2(c) shows the timing residuals for B1929+10 over the 43 yr data span from 1969 to 2012. This plot includes the JPL data spanning between 1969 and 1982 and the PRAO data spanning between 1999 and 2012. A 16 yr data gap seen in the residual curve complicates the analysis of the rotation frequency for this pulsar. Nevertheless, there are strong arguments for the existence of a change in the sign of $\ddot{\nu}$ for this pulsar.

Figure 2(c) presents the timing residuals relative to a simple ν , $\dot{\nu}$ model 1969–1982. We see that the residuals have different signatures for the two observational intervals. In the second interval over 1999–2012, the residual curve suddenly changed its slope with respect to the zero line. At the end of this interval, the deviation of the timing residuals exceeded 1000 ms, more than five pulse periods. Comparing of this plot with the plot of the timing residuals presented in Figure 3 of Hobbs et al. (2010) shows that there is good agreement between the picture of the PRAO timing residuals and that of the JBO residuals despite a 16 yr gap in our data set. In Figure 3 of Hobbs et al. (2010), we see that glitch events were absent during a 16 yr gap between 1982 and 1999. Therefore, the observed change of the slope of the residual curve is not connected with glitches. The variable character of the timing residuals is probably due to a sudden change in the conditions of the pulsar rotation.

Estimates show that a sudden change in the pulsar rotation parameters could have taken place in approximately 1997. The picture of the frequency residuals, plotted in Figure 2(d), also indicates a variable behavior of the rotation frequency. We clearly see that the $\Delta\nu$ residuals, presented relative to the timing model 1969–1982, show different structures for the two observational intervals 1969–1982 and 1999–2012.

In order to reveal the cause of the dissimilar timing behavior of PSR B1929+10 over the two intervals, we consider Figure 13. Figure 13(a) presents the timing residuals relative to the simple ν , $\dot{\nu}$ timing model 1969–1982 (on the left side) and relative to the simple ν , $\dot{\nu}$ timing model 1999–2012 (on the right side). We see that the post-fit residuals exhibit a weak cyclical structure over the first interval and a large cubic term over the second interval. The cubic term indicates a large positive value of $\ddot{\nu}$. This result means that the change of conditions in the pulsar rotation have resulted in a large $\ddot{\nu}$ value.

In the following two plots, we present evidence that a different signature of the $\Delta\nu$ residuals over the two observational intervals is due to a change in the value and the sign of the second frequency derivative $\ddot{\nu}$. Figures 13(b) and (c) display the frequency residuals $\Delta\nu$ relative to the ν , $\dot{\nu}$, $\ddot{\nu}$ timing models 1969–1982 and 1999–2012, respectively. The mean rotation parameters for these two models are given in Table 2, which clearly shows that the models include $\ddot{\nu}$ of opposite signs. Figure 13(b) shows that the $\Delta\nu$ residuals relative to the first timing model have a quasi-periodic character over the interval 1969–1982 and show a significant deviation with respect to the zero line over the second interval. A parabolic form of the $\Delta\nu$ residuals over the 1999–2012 interval indicates the presence of a large $\ddot{\nu}$, considerably exceeding $\ddot{\nu}$ of the first interval. Still greater discordance between the calculated and actual rotation frequencies is observed for another timing model, plotted in Figure 13(c). The frequency residuals $\Delta\nu$ relative to the second ν , $\dot{\nu}$, $\ddot{\nu}$ model have a noise-like character over the second interval 1999–2012 and show a very large deviation with respect to the zero line over the first interval. This result means that the calculated rotation frequencies ν cannot be compared to the actual rotation frequencies existing for the first interval. Both of these plots support a sudden change in the magnitude of $\ddot{\nu}$ between the two observational intervals.

The timing behavior of the first derivative $\dot{\nu}$ is presented in Figure 13(d). We see that the observed signature of $\dot{\nu}$ differs between the two intervals. In the second interval, the magnitude $|\dot{\nu}|$ decreases with time, indicating the presence of a large positive second derivative $\ddot{\nu}$. In this plot, the solid line indicates the best fit with a linear function.

We have presented evidence that the pulsar B1929+10 experienced a significant change in its rotation parameters between 1982 and 1999. A rapid change of the parameters ν , $\dot{\nu}$, and $\ddot{\nu}$ was accompanied by a change in the sign of $\ddot{\nu}$. This event could have taken place around 1997 (\sim MJD 50400); this year is marked by a vertical line in Figure 13.

3.2.3. Scheme of the Time Behavior of $\ddot{\nu}$ over the Observational Interval 1968–2012

The scheme of the time behavior of $\ddot{\nu}$ for two pulsars, B0823+26 and B1929+10, is plotted in Figure 14. As was shown above, the observed change in the value and the sign of $\ddot{\nu}$ is due to a rapid change of the pulsar rotation parameters ν , $\dot{\nu}$, and $\ddot{\nu}$. From this plot, we see that the time behavior of $\ddot{\nu}$ for PSR B0823+26 is well described by a rectangular function. For the other pulsar, B1929+10, the behavior of $\ddot{\nu}$ is shown by the same function. The plot suggests that we probably observe a small fragment of some long-term process that can modulate the second derivative $\ddot{\nu}$ in pulsars in such a way that the sign of $\ddot{\nu}$ is reversed. If such a modulation of $\ddot{\nu}$ is a periodical process, then the time behavior of $\ddot{\nu}$ could be described by the periodic rectangular function over long time scales. In our observations, the phenomenon of a change in the sign of $\ddot{\nu}$ is observed for two pulsars out of the 27 studied. This result means that the period of possible modulation in $\ddot{\nu}$ insignificantly exceeds the 43 yr time span of our observations by two to four times and probably reaches 100–200 yr.

So, we have revealed a phenomenon of a rapid change of the pulsar rotation parameters ν , $\dot{\nu}$, and $\ddot{\nu}$. A rapid change in the rotation frequency ν is accompanied by a distinct jump in $\dot{\nu}$ and a change in the value and the sign of $\ddot{\nu}$. The indication of the existence of such a phenomenon is that the timing behavior of the pulsar cannot be described by one ν , $\dot{\nu}$, $\ddot{\nu}$ timing model within one pulse period during a long period of observations spanning decades. For this case, two models that include $\ddot{\nu}$ values of opposite signs are required for the fitting procedure. Glitches have nothing to do with this situation.

We suppose that in the future this phenomenon—a rapid change of pulsar rotation parameters accompanied by a change in the sign of $\ddot{\nu}$ —will be revealed in the rotation frequency of many other pulsars. Figure 3 of Hobbs et al. (2010) presents the timing residuals for a sample of 366 pulsars. The large cubic trends seen in the residuals of many pulsars, presented in this plot, can have different origins. Some part of these cubic trends may result from glitch events. The other part of them may serve as indicators that these pulsars experienced a rapid change in the conditions their rotation. The cubic trend visible in the timing residuals of PSR B1929+10, shown in our Figure 13(a) over the interval 1999–2012, indicates this case.

3.3. The Evolutionary Scenario of the Occurrence of Rotational Irregularities

Figure 15 shows the relation between the measured value of the second frequency derivative $\ddot{\nu}$ and the characteristic age τ_c for the 27 studied pulsars. These parameters are listed in Table 6. We see that the plotted points form three sequences according to the signatures of

the timing residuals observed in these pulsars, as was discussed above. A detailed inspection of Figure 15 shows that certain signatures of the timing residuals are correlated with certain values of the second derivatives $\ddot{\nu}$ and certain age ranges. This correlation implies that pulsar timing irregularities have an evolutionary character. We suggest that the three plotted sequences, corresponding to different kinds of signatures in the timing residuals, indicate the three evolutionary stages of pulsar rotation. In other words, these sequences show that certain signatures in the timing residuals can occur only at a certain stage of pulsar rotation evolution. From this fact, it follows that each evolutionary stage is characterized by certain types of rotational irregularities.

3.3.1. *The Observed Types of Pulsar Rotational Irregularities*

Discrete glitches and long-term quasi-periodic oscillations. The extensive JBO timing observations and observations of other researchers have shown that phenomena such as discrete glitches and quasi-periodic processes represent two main types of rotational irregularities in pulsars (Shemar & Lyne 1996; Lyne et al. 2000; Wang et al. 2000; Hobbs et al. 2004, 2010; Yuan et al. 2010; Espinoza et al. 2011; Yu et al. 2013). Glitches occur as sudden, discrete jumps in a pulsar’s rotation frequency, followed by an exponential recovery to the pre-glitch value. Cubic trends in the timing residuals corresponding to the positive values of $\ddot{\nu}$ arise as a result of relaxation after a discrete glitch (Lyne et al. 2000). To date, a total of 422 glitches have been revealed in 138 pulsars (Espinoza et al. 2011; Yu et al. 2013). The second type of rotational irregularities occurs in the form of long-term quasi-periodic oscillations. In Figure 3 of Hobbs et al. (2010), we see that many pulsars show different quasi-periodic structures in their timing residuals. Both types of rotational irregularities can occur in the rotation frequency of one pulsar. According to Hobbs et al. (2010), the timing residuals of many pulsars represent a combination of a cubic trend and a quasi-periodic structure. From our data, this effect is clearly visible in Figure 8. The examples of quasi-periodic changes seen in the timing residuals of the pulsars in our sample are shown in Figure 9.

Slow glitches. Slow glitch phenomena present the third type of rotational irregularities. The term “slow glitch” was introduced by Shabanova (1998) to explain a glitch of an unusual, gradual signature that occurred in PSR B1822–09 over the interval 1995–1997. According to the literature, the second slow glitch in this pulsar was observed by Shabanova & Urama (2000) and the third glitch was independently observed by Zou et al. (2004) and Shabanova (2005). The oscillatory process in PSR B1822–09 was finished in 2004. Slow glitches were also investigated in detail in the rotation frequency of PSR B1642–03 and B0919+06 (Shabanova 2009b, 2010). These results showed that slow glitch

events occur in series; they produce regular oscillations in a pulsar’s rotation frequency that looks like a continuous sequence of glitch-like events. These oscillations in the rotation frequency give rise to rapid, regular oscillations in the timing residuals. As reported by Yuan et al. (2010), slow glitches have yet to be identified for two pulsars, J0631+1036 and B1907+10. An extension of this work would be to study the properties of these events and to find evidence that they are glitch events, rather than timing noise. According to Hobbs et al. (2010), slow glitches are not a unique phenomenon and they can be caused by the same process that causes timing noise in pulsars. Another point of view was suggested by Yu et al. (2013). These authors proposed that it is reasonable to label as slow glitches the observed discrete events that result in quasi-sinusoidal features in the timing residuals. This fact means that the idea of slow glitches has received confirmation from Yu et al. (2013).

Apparently, the phenomenon of slow glitches is not widespread among pulsars. A sample of 10 pulsars whose timing residuals demonstrate a regular cyclical structure is shown in Figure 1 of Lyne et al. (2010). According to a model proposed by these authors, these timing data are explained by quasi-periodic switching in the spin-down rate of these pulsars. As discussed by Jones (2012), the harmonic structure seen in the timing residuals of these 10 pulsars is consistent with the precession interpretation. We suppose that most pulsars from this sample are candidates for having slow glitches in their rotation frequencies.

It should be noted that regular oscillations were observed earlier in the rotation rate of the Crab pulsar from JBO observations over the interval 1982–1989. The period of a regular component of the timing residuals was estimated to be ~ 20 months (Lyne et al. 1988) or 568 ± 10 days (Scott et al. 2003). Lyne et al. (1988) claimed that the observed cyclical residuals with this period were consistent with a physically real quasi-periodic process. In our opinion, the periodic process with the 568 days period observed in the Crab pulsar resembles the phenomenon of slow glitches producing a periodic sawtooth-like modulation with a period of 600 days in the timing residuals of the pulsar B0919+06 (Shabanova 2010).

It is quite possible that the phenomenon of slow glitches presents an intermediate position between discrete glitches and quasi-periodic processes. On the one hand, slow glitch events show properties that should characterize them as discrete glitch events. For example, a linear relation between the amplitudes of glitches and the post-glitch intervals was revealed both for the X-ray pulsar J0537–6910 (Middleditch et al. 2006) and for the pulsar B1642–03 (see Figure 3 of Shabanova (2009b)). On the other hand, a sequence of slow glitches produces regular cyclical changes in the timing residuals. Regular oscillations may be a particular case of more general phenomenon related to long-term quasi-periodic oscillations observed in the rotation rate of many pulsars. In any case, the phenomenon of slow glitches is due to real oscillatory processes rather than random variations in the pulsar

rotation rate.

A phenomenon of a sudden change in the sign of the second derivative $\ddot{\nu}$. In Section 3.2, we reported the detection of a new phenomenon that is associated with a change of pulsar rotation parameters ν , $\dot{\nu}$, and $\ddot{\nu}$. These parameters change in such a way that the sign of $\ddot{\nu}$ is reversed, as is shown in Figure 14. This phenomenon was detected in the timing behavior of two pulsars, B0823+26 and B1929+10. It is very likely that a similar rapid change of rotation parameters can occur in many other pulsars. If such a process cycles in time, then it can be considered a modulation process. A rough estimate shows that a change of rotation parameters can occur in the rotation rate of some pulsars about once every 100 yr. The sign of $\ddot{\nu}$ will change to the opposite sign with the same interval. This process can be a candidate to represent the fourth type of rotational irregularities.

3.3.2. Rotational Irregularities in the First Stage of Pulsar Rotation Evolution

In Figure 15, we see that the pulsars that show cubic components in their timing residuals (marked by solid circles) can be thought of as being in the first stage of pulsar rotation evolution. These pulsars have large values of $\ddot{\nu}$ with both signs and are the youngest pulsars in our sample. The given sequence of pulsars also includes two pulsars, B0823+26 and B1929+10 (marked by squares), whose timing behavior is determined by a rapid change of the rotation parameters and a change in the sign of $\ddot{\nu}$. In Figure 8, we see that all these pulsars also have a quasi-periodic structure seen in their timing residuals after the removal of a cubic trend from the arrival times. At the first stage, there are also slow glitch events. As was discussed above, two pulsars from the first group, B1822–09 and B0919+06, show a regular cyclical structure in their timing residuals which are due to slow glitches.

We conclude that rotational irregularities in the first stage of pulsar rotation evolution are produced by such phenomena as discrete glitches, slow glitches, quasi-periodic processes, and processes of a rapid change of pulsar rotation parameters.

3.3.3. Rotational Irregularities in the Second Stage of Pulsar Rotation Evolution

Figure 15 shows that the pulsars that stay in the second stage of pulsar rotation evolution (marked by star symbols) show timing residuals that are dominated by quasi-periodic components. These pulsars are older pulsars, although their age partially overlaps with the ages of the pulsars remaining in the first stage. These pulsars also have considerably smaller measured $\ddot{\nu}$ values. The timing residuals of these pulsars exhibit a great variety of quasi-

periodic structures, as is seen in Figures 2 and 9. Besides quasi-periodic processes, small discrete glitches and slow glitches can also occur in the rotation frequency of these pulsars. For example, the cyclical timing residuals of PSR B1642–03 are due to the presence of slow glitches. As discussed above, the pulsar B2217+47 experienced a small discrete glitch of magnitude $\Delta\nu/\nu \sim 1.3 \times 10^{-9}$ that occurred in 2011 October. It is very likely that in the second stage of rotation evolution, events such as large discrete glitches already will not occur. The process of rapid changes of pulsar rotation parameters also disappears.

We conclude that rotational irregularities in the second stage of pulsar rotation evolution are produced by such phenomena as quasi-periodic processes, small discrete glitches, and slow glitches. These processes are the cause of measurable values of $\ddot{\nu}$ for these pulsars.

3.3.4. Rotational Irregularities in the Third Stage of Pulsar Rotation Evolution

The third group (marked by triangle symbols) includes pulsars whose timing residuals exhibit noise-like variations. In Figure 15, we see that the ages of these pulsars almost completely overlaps with the ages of the pulsars remaining in the second stage. This result indicates that pulsars of the same age can remain in different stages of rotation evolution.

The pulsars that belong to the third stage of pulsar rotation evolution have many properties in common (see Figure 11). The periods of these pulsars usually are more than one second. The timing residuals mainly are due to measurement errors, although some pulsars of this group can show a weak remnant structure, as in the case of PSR B1839+56. In Figure 15, we see that the measured $\ddot{\nu}$ values for these pulsars are on the boundary of the precision of our measurements, which is equal to $1 \times 10^{-28} \text{ s}^{-3}$. The limited span of timing data does not allow us to measure the deterministic $\ddot{\nu}$ values, which for most pulsars from this group should be less than 10^{-29} s^{-3} .

We conclude that rotational irregularities in the third stage of pulsar rotation evolution should gradually disappear. At this stage in the timing residuals, noise-like variations dominate. It follows that in the future these pulsars will never be observed to glitch.

3.3.5. The Age Ranges in the Three Stages of Pulsar Rotation Evolution

An analysis of the data, plotted in Figure 15, shows that the age boundaries between different evolutionary stages are indistinct and diffusive. This result implies that the rotation rates of pulsars of the same age can evolve along different paths. In Figure 15 and Table 6, we see that the middle-aged pulsar B0834+06 is approximately the same age as the pulsars

B2217+47 and B1929+10. In contrast to these pulsars, B0834+06 stays in the third stage of pulsar rotation evolution. This example illustrates that pulsars of the same age can have different evolution rotation histories.

From Figure 15, we may estimate the age range for each evolutionary stage. The younger pulsars from our sample with characteristic ages between 10^5 and 10^7 yr belong to the first evolutionary stage. The second stage includes the middle-aged pulsars with ages greater than $\sim 10^6$ yr. The third evolutionary stage includes both the middle-aged and old pulsars but the middle-aged pulsars in the third stage exhibit much less timing noise than pulsars of the same age in the second evolutionary stage. The uncertainty of the age boundaries between different evolutionary stages complicates the correlation between the amount of timing noise and pulsar age.

A detailed inspection of Figure 15 shows that rotation rates of pulsars do not always pass through all three evolutionary stages. Some pulsars can stay in the first stage during their whole lives. On the contrary, some pulsars can escape the first stage of rotation evolution if they never experience large glitches. Pulsars that have stable rotation over their whole lives can at once fall into the third evolutionary stage. The last feature of rotation evolution implies that, despite the limited accuracy of our measurements, the deterministic values of $\ddot{\nu}$ can be measured for some middle-aged pulsars that stay in the third evolutionary stage. Among these pulsars, there will always be pulsars that did not experience any shocks in their life and consequently have stable rotation and a low level of timing noise.

For example, we examine the pulsar B0834+06. This middle-aged pulsar has a relatively low level of timing noise, as discussed above (see Figure 2(c)). We may suppose that neither discrete glitches nor quasi-periodic oscillations disturbed the rotation of this pulsar during its life. Figure 15 shows that the measured $\ddot{\nu}$ value for this pulsar falls very close to the sloping line of the deterministic values of $\ddot{\nu}$, indicating that slowdown of the rotation of this pulsar is closely related to a simple $\nu, \dot{\nu}$ spin-down model. We conclude that a measurement of the deterministic value of $\ddot{\nu}$ for this pulsar is possible in the near future rather than in hundreds of years as for the other older pulsars.

3.3.6. *The Magnetic Fields in the Three Stages of Pulsar Rotation Evolution*

Evolution of the magnetic field of a neutron star was discussed in detail in a series of papers (Ruderman 1991a,b, 2004, 2006; Ruderman et al. 1998). We consider the evolutionary picture of the magnetic field for the middle-aged and old pulsars taking into account the signatures of the timing residuals observed in these pulsars. Figure 16(a) shows the

dependence of the surface magnetic field strength B_s on the characteristic age τ_c for the 27 studied pulsars. The parameters B_s and τ_c are listed in Table 6. The three plotted sequences indicate that the magnetic field values B_s considerably differ for the three groups of pulsars and that these values are furthermore correlated with certain signatures of the timing residuals. Here, a sequence of the B_s values for the pulsars with cubic signatures of the timing residuals is marked by solid circles, pulsars with quasi-periodic signatures in their residuals are marked by star symbols, and pulsars with noise-like signatures in their residuals are marked by triangle symbols.

We see two surprising features in the observed correlation picture. First, the B_s values of the pulsars showing noise-like components in their timing residuals (the B_{nois} values), is greater than the B_s values of the pulsars of the same age that show timing residuals dominated by cubic components (the $B_{(cub)}$ values) or quasi-periodic components (the $B_{(cyc)}$ values). This result may mean that magnetic fields are stronger for pulsars whose rotation is more stable.

Second, a sequence of $B_{(cyc)}$ values continues well into a sequence of the $B_{(cub)}$ values. This result indicates a common evolutionary path for these two groups of pulsars. For analysis, these two sequences are combined into one sequence $B_{(cub+cyc)}$, as is shown in Figure 16(b). We see that the two straight lines fit to the sequences of $B_{(nois)}$ points and $B_{(cub+cyc)}$ points have identical slopes. For pulsars of the same age, the $B_{(nois)}$ values nearly four times greater than the $B_{(cub+cyc)}$ values. This result suggests that the magnetic fields are approximately four times stronger for the pulsars that have stable rotation. The dependence of the B_s values on different kinds of signatures of the timing residuals is a good indication of the validity of the supposition that the rotation rates of pulsars pass through different evolutionary stages and that some pulsars can have a special path of evolution that is characterized by a very stable pulsar rotational behavior during the whole pulsar’s life. We conclude that the observed correlation picture of the surface magnetic field strength B_s with certain signatures of the timing residuals, presented in Figure 16, provides convincing evidence for the existence of the evolutionary scenario of the origin of rotational irregularities.

In order to check the results obtained above for a large number of pulsars, we analyzed the JBO timing residuals, presented in Figure 3 of Hobbs et al. (2010). We tried to classify ordinary pulsars of middle and older age according to the signatures of their timing residuals. The obtained results are shown in Figure 17. Figure 17(a) displays a relation between the measured values of $\ddot{\nu}$ and the characteristic age τ_c . Here, 73 selected pulsars showing timing residuals dominated by cubic and quasi-periodic components are marked by squares and 64 pulsars showing noise-like components in their timing residuals are marked by open circles. The plotted three sequences present the PRAO data, as in Figure 15. We see that the

distribution of the plotted points does not contradict the supposition about the existence of three stages of pulsar rotation evolution.

Figure 17(b) displays the relation between the surface magnetic field strength B_s and τ_c for the selected pulsars from the JBO sample. The plotted two sequences present the PRAO data, as in Figure 16(b). In this plot, the two straight lines fit to two groups of JBO points show that magnetic fields are stronger for pulsars exhibiting noise-like signatures in their timing residuals. This result confirms that pulsars that stay in the third evolutionary stage have a tendency to show stronger magnetic fields than pulsars in other stages. We conclude that the evolutionary scenario of the occurrence of rotational irregularities is confirmed by the dependencies that are presented in Figure 17 for a large number of pulsars.

4. Discussion

4.1. Explanation of the Large Values of $\ddot{\nu}$ with Both Signs

We suppose that the large values of $\ddot{\nu}$ with both signs are the result of the existence of four types of rotational irregularities that have evolutionary characteristics and form three evolutionary stages in pulsar rotation rate. Rotational irregularities alone are responsible for the large values of the measured second derivative $\ddot{\nu}$ and the variable structure of the timing noise over a long time scale.

As discussed above, rotational irregularities occur in the form of discrete glitches, quasi-periodic oscillatory processes, slow glitches, and processes that change the pulsar rotation parameters ν , $\dot{\nu}$, and $\ddot{\nu}$ in such a way that the sign of $\ddot{\nu}$ is reversed. An analysis of timing noise showed that several types of rotational irregularities can simultaneously occur in the rotation rate of one pulsar. For example, the rotation frequency of PSR B0919+06 over the interval 1979–2009 underwent large changes that were due to three types of rotational irregularities including a series of 19 slow glitches, a long-term quasi-periodic process, and a large discrete glitch (Shabanova 2010). We conclude that rotational irregularities are the cause of the deviation of the timing behavior of most pulsars from a simple ν , $\dot{\nu}$ model. This conclusion is in accordance with the statement by Hobbs et al. (2010) that the timing noise cannot be explained by models that are based on random walks in the pulse phase, frequency, or spin-down rate. Such models are not consistent with the observations.

It is known that the $\ddot{\nu}$ values for the simple model of magnetic dipole braking should be positive. However, timing observations show that pulsars with characteristic ages more than $\tau_c > 10^5$ yr have both the positive and negative $\ddot{\nu}$ values. As pointed out by Hobbs et al. (2010), approximately 52% of these pulsars have a positive $\ddot{\nu}$ value and 48% have negative $\ddot{\nu}$.

These authors noted that this situation is not related to glitch recovery nor magnetic dipole radiation, but is a result of some other process.

We propose that we have found a process that can result in a change in the sign of $\ddot{\nu}$ in pulsars. As was reported in Section 3.2, this process changes the pulsar rotation parameters together with a change in the sign of $\ddot{\nu}$, as shown in Figure 14. This process was detected in the timing behavior of two pulsars, B0823+26 and B1929+10. It is very likely that a similar rapid change of rotation parameters can occur in many other pulsars. If so, then this process could explain the problem that approximately equal numbers of pulsars have timing residuals in the form of a cubic polynomial with positive (20%) and negative (16%) signs of $\ddot{\nu}$ (Hobbs et al. 2010). While glitch recovery produces cubic trends corresponding to the positive values of $\ddot{\nu}$, this process could cause large values of $\ddot{\nu}$ with both signs. It should be noted that such a process apparently can operate only in pulsars that stay in the first stage of pulsar rotation evolution. In the final stages of rotation evolution, negative signs of $\ddot{\nu}$ can result from the limited temporal baseline of data of a more long-term oscillatory process.

In the literature, there are different interpretations of the origin of large $\ddot{\nu}$ values. In the paper by Urama et al. (2006), the large values of $\ddot{\nu}$ with both signs are attributed to small variations in the spin-down torque. Biryukov et al. (2012) discussed this problem in the context of the pulsar spin-down model that involves the existence of a long-term cyclical process changing the observed rotation parameters. This cyclical process is superimposed on the secular spin-down of pulsars and produces cyclical variations in $\ddot{\nu}$ with time scales of a few thousand years. The second interpretation is in accordance with our experimental result describing the fourth type of rotational irregularities. This type of irregularity produces a change in the sign of $\ddot{\nu}$ owing to a rapid change of pulsar rotation parameters. However, we explain the origin of the large $\ddot{\nu}$ values and the variable structure of the timing noise by the existence of four types of rotational irregularities that have evolutionary characteristics.

4.2. Explanations for Other Observed Properties of Pulsar Rotation

We propose an evolutionary scenario for the occurrence of rotational irregularities to explain the observed properties of timing noise in pulsars. Timing noise is common among pulsars because rotational irregularities occur in pulsars of all ages, but the strength of timing noise depends on the evolutionary stage of pulsar rotation, as is shown in Figure 15. Younger pulsars stay in the first evolutionary stage of pulsar rotation where the pulsar rotation frequency is subject to all four types of rotational irregularities—discrete glitches, quasi-periodic oscillations, slow glitches, and processes that change pulsar rotation parameters, and, as a consequence, change the sign of $\ddot{\nu}$. These pulsars have the largest $\ddot{\nu}$ values and

show strong timing noise. In their timing residuals a large cubic trend dominates that is the result of relaxation after a discrete glitch (for $\dot{\nu} > 0$) or the result of a process of a change in the sign of $\dot{\nu}$ (for $\dot{\nu}$ with both signs). The middle-aged pulsars stay in the second evolutionary stage of pulsar rotation and their timing activity is related to three types of rotational irregularities—quasi-periodic oscillations, slow glitches, and small discrete glitches. The timing residuals of such pulsars exhibit mainly a quasi-periodic character. The strength of the timing noise of old pulsars that stay in the third evolutionary stage weakens because rotational irregularities at this stage gradually disappear. The timing residuals of old pulsars are mainly dominated by noise-like variations. This presented evolutionary picture is in accordance with the results of Hobbs et al. (2010), who discussed the features of timing residuals depending on the characteristic age of pulsars.

The age boundaries between different evolutionary stages are diffusive. This feature of pulsar rotation evolution explains why two pulsars with similar rotation parameters exhibit different signatures in their timing residuals. For example, two pulsars, B0943+10 and B1133+16, have almost identical rotation parameters ν and $\dot{\nu}$, as follows from Table 2, but exhibit different structures in their timing and frequency residuals, as seen in Figures 2(c) and 2(d). This result occurs because these pulsars have different evolutionary histories; they evolve along different paths and therefore belong to different evolutionary stages of pulsar rotation. In Figure 15, we see that the pulsar B0943+10 stays in the first evolutionary stage, while the pulsar B1133+16 stays in the second stage of pulsar rotation evolution.

It was believed that all pulsars can experience glitches (Alpar & Baykal 1994, 2006; Melatos et al. 2008). The evolutionary scenario for the origin of pulsar rotational irregularities is inconsistent with this statement. Pulsar glitches are not common phenomena experienced by pulsars of all ages. Figure 15 shows that pulsar glitches occur more frequently in younger pulsars as these pulsars belong to the first evolutionary stage of pulsar rotation. Pulsar glitches will never occur in old pulsars that belong to the third evolutionary stage of pulsar rotation. Pulsars in the final evolutionary stage either already have experienced the stage of glitches in their rotation rate or have never experienced any shocks in their life and so immediately entered the final stage of pulsar rotation evolution. As a consequence, one pulsar may regularly experience glitch events while another pulsar with similar properties has never been observed to glitch.

5. Summary

On the basis of a detailed analysis of the timing behavior of 27 pulsars over long data baselines spanning up to 43.5 yr, we have revealed the following important features of pulsar

rotation.

1. We detected a new type of rotational irregularity that is the result of a rapid change of pulsar rotation parameters in such a way that the sign of $\ddot{\nu}$ is reversed. This process was revealed in the timing behavior of two pulsars, B0823+26 and B1929+10. The detected phenomenon of changing the sign of $\ddot{\nu}$ can help to explain the problem why pulsars with characteristic ages older than $\tau_c > 10^5$ yr have both positive and negative $\ddot{\nu}$ values.

2. We showed that a variable structure of timing noise over long time scales is produced by four types of rotational irregularities that occur in the form of discrete glitches, quasi-periodic oscillations, slow glitches, and a process changing pulsar rotation parameters together with a change in the sign of $\ddot{\nu}$.

3. We found that all four types of observed rotational irregularities have evolutionary nature and form three evolutionary stages in pulsar rotation rate. This result means that a certain type of rotational irregularity can occur only at a certain stage of pulsar rotation evolution. In the first stage of rotation evolution, including the younger pulsars with $\tau_c < 10^7$ yr, all four types of rotational irregularities occur—discrete glitches, slow glitches, quasi-periodical oscillations, and a process of changing pulsar rotation parameters and the sign of $\ddot{\nu}$. In the second stage of rotation evolution, including the middle-aged pulsars with $\tau_c > 10^6$ yr, large glitches and the process that changes the sign of $\ddot{\nu}$ disappear. Rotational irregularities include only small discrete glitches, slow glitches, and quasi-periodical oscillations. In the third stage of rotation evolution, including both the middle-aged and old pulsars, rotational irregularities should gradually weaken and disappear entirely. In this stage, the timing residuals are mainly dominated by noise-like variations. The evolutionary nature of rotation irregularities indicates that the deterministic values of $\ddot{\nu}$ and accordingly to the true values of the braking indices n can be never measured for ordinary pulsars that stay in the first or second stages of pulsar rotation evolution.

4. We found that the surface magnetic field strength B_s for pulsars is correlated with certain signatures of the timing residuals, as shown in Figure 16. We revealed two surprising features in this correlation picture. The first feature is that the magnetic fields are stronger for pulsars that show noise-like signatures in their timing residuals, that is, for the pulsars whose rotation has a more stable character. The second feature is that the magnetic fields for two groups of the pulsars, those exhibiting timing residuals with cubic signatures and those exhibiting timing residuals with quasi-periodic signatures, smoothly vary from one group to another. This result indicates that these two groups of pulsars have a common evolutionary path. The observed correlation of the magnetic field with certain signatures of the timing residuals confirms the evolutionary nature of rotational irregularities.

5. We found that the age boundaries between different evolutionary stages are indistinct and diffusive. This result is because different pulsars with similar properties evolve along different paths and have different evolutionary histories. The first corollary of this feature is that pulsar glitches are not a common event experienced by pulsars of all ages. Pulsar glitches will never occur in old pulsars that belong to the third evolutionary stage of pulsar rotation. The second corollary of this feature is that the measurements of the deterministic values of $\dot{\nu}$ are possible for some middle-aged pulsars that stay in the third evolutionary stage and show stable rotation and a low level of timing noise. It is very likely that these pulsars did not experience any shocks over their lifetimes. Then, the measurements of the deterministic $\dot{\nu}$ values for such pulsars will not require very long, in hundreds of years, data baselines.

6. We detected a small glitch in the pulsar B2217+47. The glitch occurred in 2011 October 24 (MJD 55858) and was characterized by a fractional increase in the rotation frequency of $\Delta\nu/\nu \sim 1.3 \times 10^{-9}$.

7. We showed that there are arguments in favor of the existence of continuous changes in the DM over the interval 1999–2007 for the pulsar B2224+65.

In summary, we have studied the properties of the timing behavior of 27 pulsars whose characteristic ages range from 10^5 to 10^8 yr. We propose that the evolutionary scenario of the occurrence of rotational irregularities can be generalized to all ordinary pulsars in the given age range. Very likely, the timing residuals of younger pulsars can also be well explained in the context of the evolutionary scenario of the occurrence of rotational irregularities.

We are grateful to R. D. Dagkesamansky for discussions and valuable comments and the staff of the PRAO for their aid in carrying out the many-year pulsar observations on the BSA radiotelescope. This work was supported by the Russian Foundation for Basic Research (grant No. 09-02-00473) and the Program of the Russian Academy of Sciences Physical Division "Active Processes in Galactic and Extragalactic Objects". The authors are grateful to the referee for helpful comments and suggestions.

REFERENCES

- Alpar, M. A., & Baykal, A. 1994, MNRAS, 269, 849
- Alpar, M. A., & Baykal, A. 2006, MNRAS, 372, 489
- Arzoumanian, Z., Nice, D. J., Taylor, J. H., & Thorsett, S. E. 1994, ApJ, 422, 671

- Backus, P. R., Taylor, J. H., & Damashek, M. 1982, *ApJL*, 255, L63
- Baykal, A., Alpar, M. A., Boynton, P. E., & Deeter, J. E. 1999, *MNRAS*, 306, 207
- Biryukov, A., Beskin, G., & Karpov, S. 2012, *MNRAS*, 420, 103
- Boynton, P. E., Groth, E. J., Hutchinson, D. P., et al. 1972, *ApJ*, 175, 217
- Chatterjee, S., & Cordes, J. M. 2004, *ApJL*, 600, L51
- Cordes, J. M., & Downs, G. S. 1985, *ApJS*, 59, 343
- Cordes, J. M., & Helfand, D. J. 1980, *ApJ*, 239, 640
- D’Alessandro, F., McCulloch, P. M., Hamilton, P. A., & Deshpande, A. A. 1995, *MNRAS*, 277, 1033
- Demianski, M., & Proszynski, M. 1979, *Natur*, 282, 383
- Downs, G. S., & Krause-Polstorff, J. 1986, *ApJS*, 62, 81
- Downs, G. S., & Reichley, P. E. 1983, *ApJS*, 53, 169
- Espinoza, C. M., Lyne, A. G., Stappers, B. W., & Kramer, M. 2011, *MNRAS*, 414, 1679
- Gullahorn, G. E., & Rankin, J. M. 1982, *ApJ*, 260, 520
- Helfand, D. J., Taylor, J. H., Backus, P. R., & Cordes, J. M. 1980, *ApJ*, 237, 206
- Hobbs, G., Lyne, A. G., & Kramer, M. 2010, *MNRAS*, 402, 1027
- Hobbs, G., Lyne, A. G., Kramer, M., Martin, C. E., & Jordan, C. 2004, *MNRAS*, 353, 1311
- Janssen, G. H., & Stappers, B. W. 2006, *A&A*, 457, 611
- Jones, D. I. 2012, *MNRAS*, 420, 2325
- Konacki, M., Lewandowski, W., Wolszczan, A., Doroshenko, O., & Kramer, M. 1999, *ApJL*, 519, L81
- Livingstone, M. A., Kaspi, V. M., Gavriil, F. P., & Manchester, R. N. 2005, *ApJ*, 619, 1046
- Lyne, A., Hobbs, G., Kramer, M., Stairs, I., & Stappers, B. 2010, *Sci*, 329, 408
- Lyne, A. G. 1987, *Natur*, 326, 569

- Lyne, A. G. 1996, in IAU Colloq. 160, Pulsars: Problems and Progress, ed. S. Johnston, M. A. Walker, & M. Bailes (San Francisco, CA: ASP), 73
- Lyne, A. G., Pritchard, R. S., & Smith, F. G. 1988, MNRAS, 233, 667
- Lyne, A. G., Shemar, S. L., & Smith, F. G. 2000, MNRAS, 315, 534
- Manchester, R. N., Hobbs, G. B., Teoh, A., & Hobbs, M. 2005, AJ, 129, 1993
- Manchester, R. N., & Taylor, J. H. 1974, ApJL, 191, L63
- Manchester, R. N., & Taylor, J. H. 1977, Pulsars (San Francisco, CA: Freeman)
- Melatos, A., Peralta, C., & Wyithe, J. S. B. 2008, ApJ, 672, 1103
- Middleditch, J., Marshall, F. E., Wang, Q. D., Gotthelf, E. V., & Zhang, W. 2006, ApJ, 652, 1531
- Ruderman, M. 1991a, ApJ, 382, 576
- Ruderman, M. 1991b, ApJ, 382, 587
- Ruderman, M. 2004, arXiv:astro-ph/0410607
- Ruderman, M. 2006, arXiv:astro-ph/0610375
- Ruderman, M., Zhu, T., & Chen, K. 1998, ApJ, 492, 267
- Scott, D. M., Finger, M. H., & Wilson, C. A. 2003, MNRAS, 344, 412
- Shabanova, T. V. 1990, SvA, 34, 372
- Shabanova, T. V. 1995, ApJ, 453, 779
- Shabanova, T. V. 1998, A&A, 337, 723
- Shabanova, T. V. 2005, MNRAS, 356, 1435
- Shabanova, T. V. 2007, Ap&SS, 308, 591
- Shabanova, T. V. 2009a, ARep., 53, 465
- Shabanova, T. V. 2009b, ApJ, 700, 1009
- Shabanova, T. V. 2010, ApJ, 721, 251
- Shabanova, T. V., Lyne, A. G., & Urama, J. O. 2001, ApJ, 552, 321

- Shabanova, T. V., & Urama, J. O. 2000, *A&A*, 354, 960
- Shemar, S. L., & Lyne, A. G. 1996, *MNRAS*, 282, 677
- Taylor, J. H., Manchester, R. N., & Lyne, A. G. 1993, *ApJS*, 88, 529
- Urama, J. O., Link, B., & Weisberg, J. M. 2006, *MNRAS*, 370, L76
- Wang, N., Manchester, R. N., Pace, R. T., et al. 2000, *MNRAS*, 317, 843
- Yu, M., Manchester, R. N., Hobbs, G., et al. 2013, *MNRAS*, 429, 688
- Yuan, J. P., Wang, N., Manchester, R. N., & Liu, Z. Y. 2010, *MNRAS*, 404, 289
- Zou, W. Z., Wang, N., Wang, H. X., et al. 2004, *MNRAS*, 354, 811

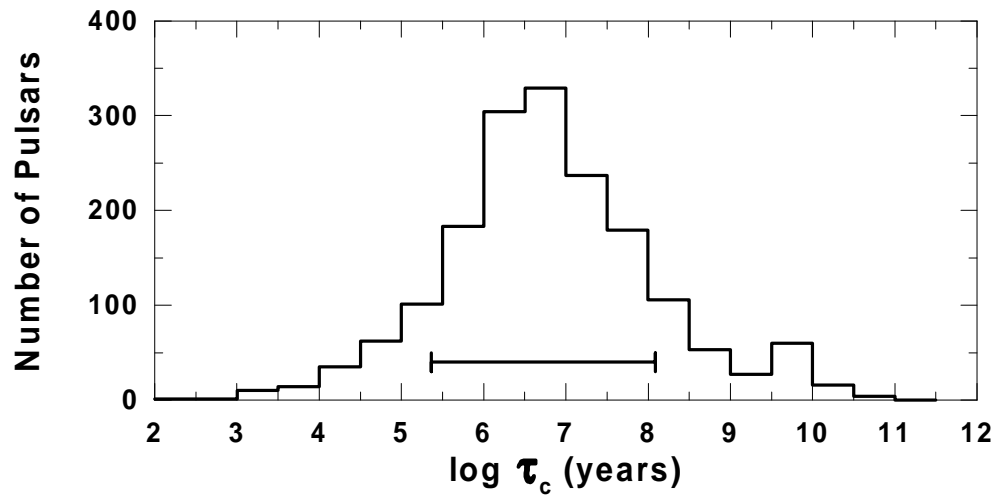


Fig. 1.— Histogram of characteristic ages of known pulsars based on the ATNF Pulsar Catalogue. The age range of the 27 pulsars from the PRAO sample is indicated by the horizontal line. We see that nearly 80% of the general pulsar population has ages within this range.

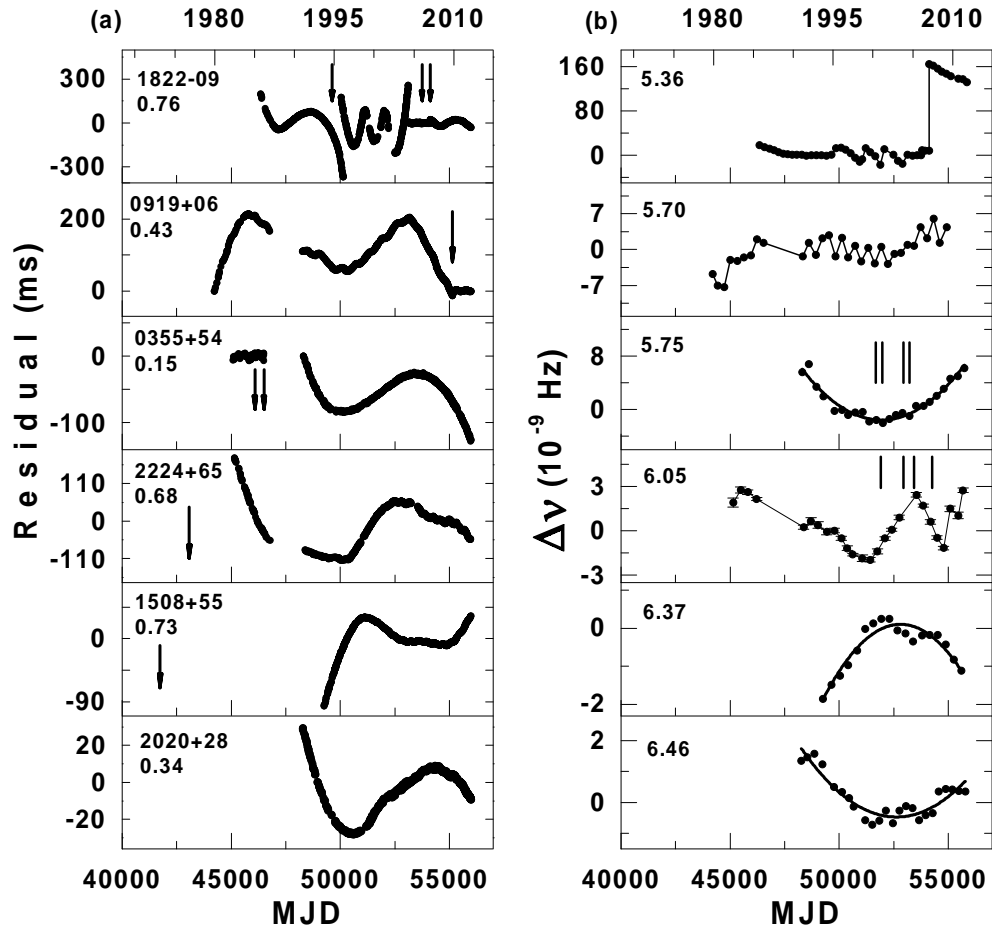


Fig. 2.— Timing behavior of 27 pulsars between 1968 and 2012. (a and b) The left-hand panel shows the timing residuals relative to a simple ν , $\dot{\nu}$ spin-down model. The glitch epochs are marked by arrows. The right-hand panel shows the corresponding frequency residuals $\Delta\nu$. The epochs of micro-glitches with a size of $\Delta\nu/\nu \sim 10^{-10}$ to 10^{-11} are marked by vertical lines. A parabolic solid curve marks the best fit with a parabolic function. All the plots are arranged in order of increasing characteristic age of the pulsars. The pulsar B1950 name and the pulse period (seconds) are indicated in each left-hand panel. Pulsar age (years) is indicated on a logarithmic scale in each right-hand panel. Error bars in the $\Delta\nu$ residuals are shown in those panels, when they are larger than the plotted points.

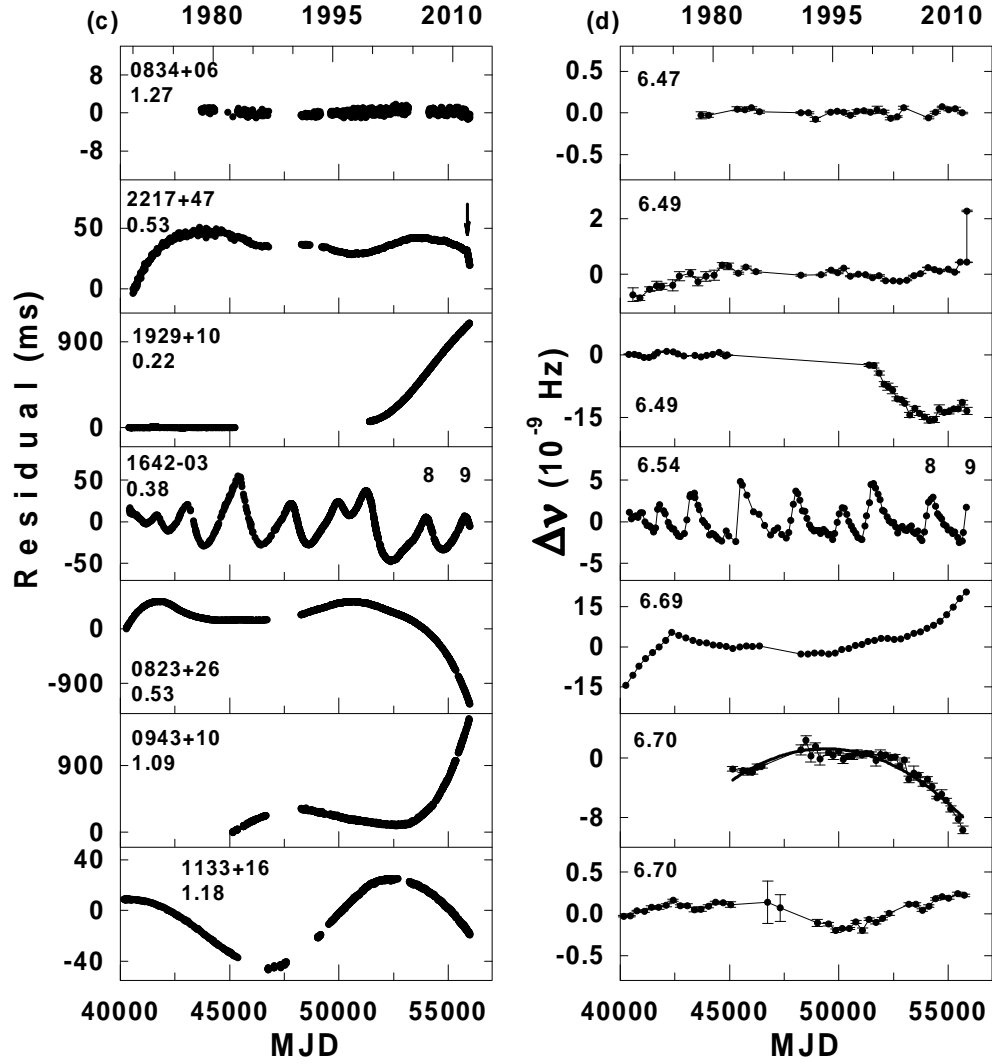


Fig. 3.— Figure 2-continued. (c and d) In the panel of PSR B2217+47, an arrow marks the epoch of the glitch that occurred in 2011 October 24 (MJD 55858). The corresponding $\Delta\nu$ plot shows that this glitch has a small absolute amplitude of $\Delta\nu \sim 2.3 \times 10^{-9}$ Hz. In the panel of PSR B1642–03, a sequence of slow glitches includes eight slow glitches and shows a new, ninth glitch seen at the very end of the data set.

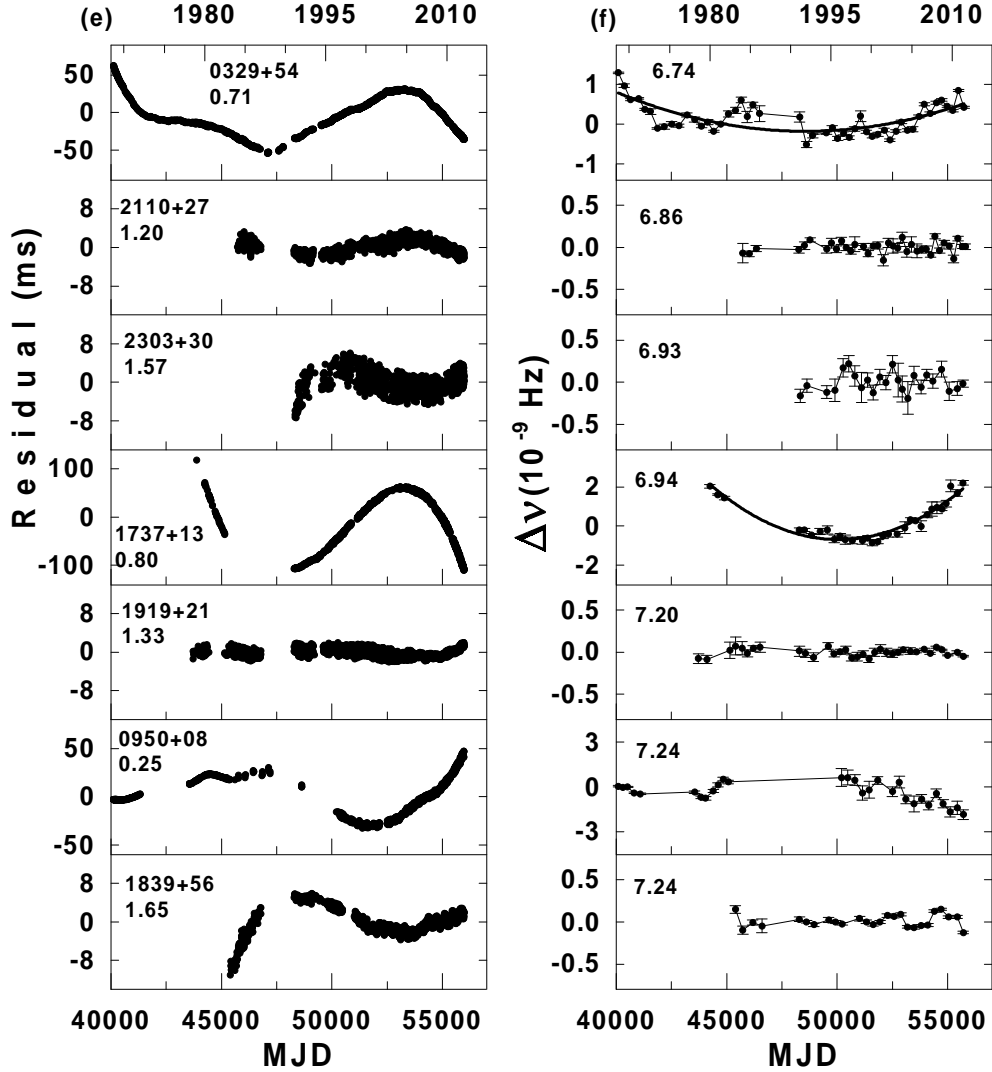


Fig. 4.— Figure 2-continued. (e and f) In the panel of PSR B0329+54, it is seen that the first half of the timing residuals contains the long-term cyclical variation that is superimposed on an appreciable cubic trend. The parabolic character of the corresponding $\Delta\nu$ residuals indicates that a significant $\ddot{\nu}$ dominates in the residuals during the whole interval of observations despite a noticeable quasi-sinusoidal structure visible in the first half of the $\Delta\nu$ curve.

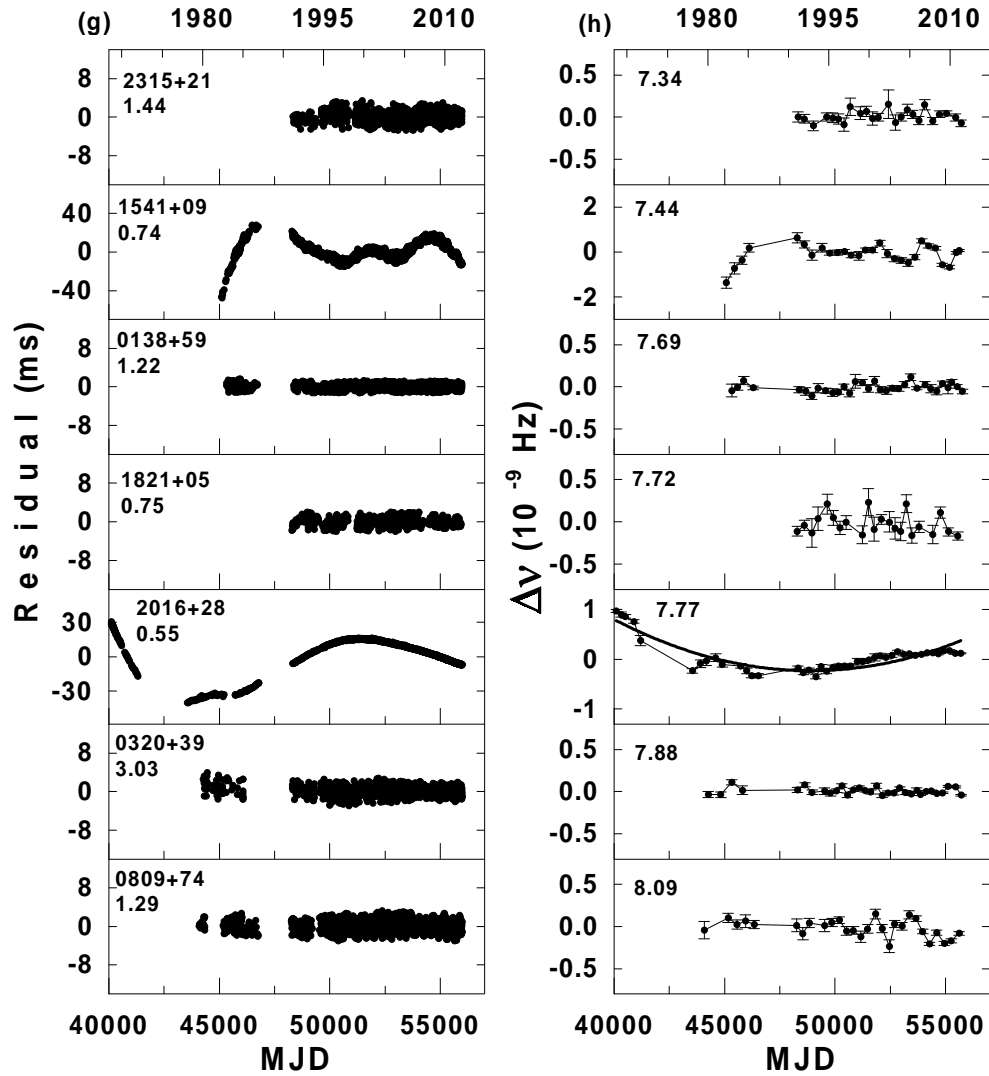


Fig. 5.— Figure 2-continued. (g and h) In the panel of PSR B1541+09, the timing residuals show two cycles of a clear quasi-sinusoidal structure visible over the interval 1995–2011.

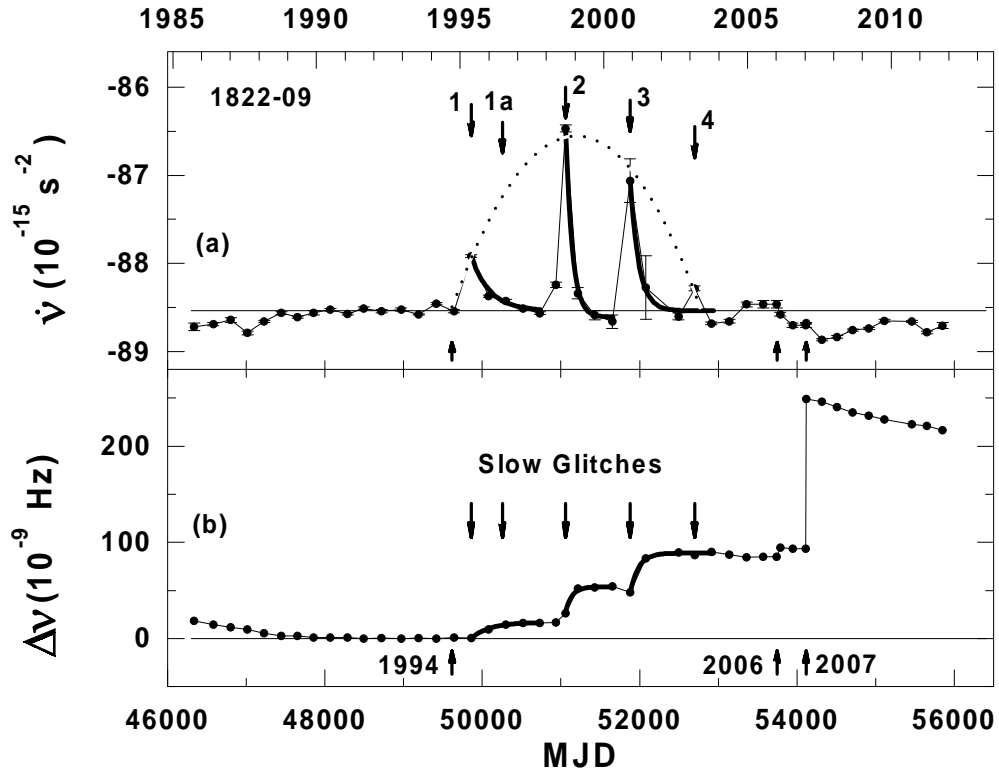


Fig. 6.— Five slow glitches and three discrete glitches in PSR B1822–09. Arrows pointing downward indicate the epochs at which the slow glitches occurred while arrows pointing upward indicate the discrete glitches. (a) The changes of $\dot{\nu}$ over the 1995–2004 interval are due to the slow glitches. We see that the $\Delta\dot{\nu}$ peaks lie on a parabolic curve that is the envelope of these peaks. (b) The $\Delta\nu$ residuals relative to a simple $\nu, \dot{\nu}$ model 1991–1994. The gradual increase in $\Delta\nu$ over the 1995–2004 interval is due to the slow glitches. The exponential fits to the $\dot{\nu}$ curve and the $\Delta\nu$ curve are drawn with bold lines in panels (a) and (b). The signature of the large glitch of 2007 is clearly seen on the right side of the $\Delta\nu$ plot.

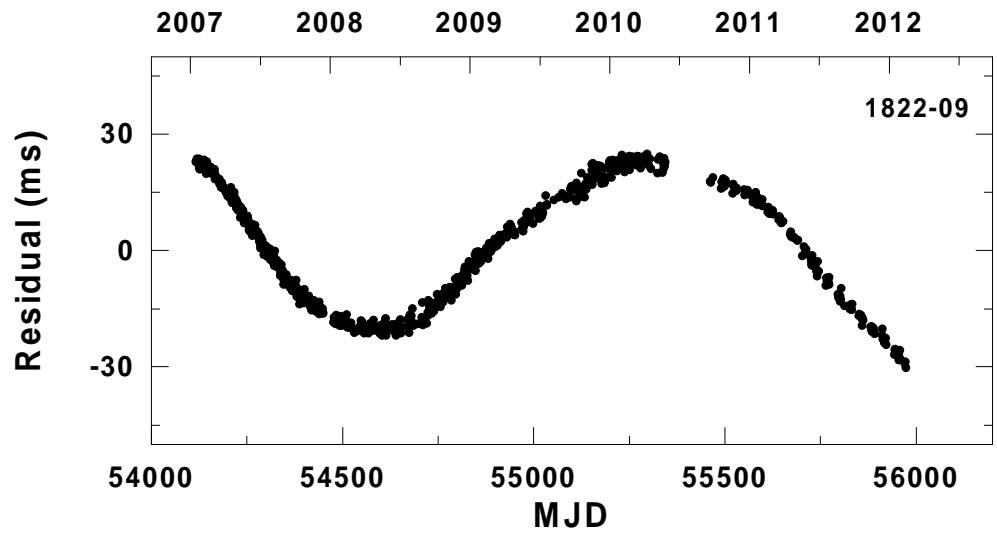


Fig. 7.— Timing residuals for PSR B1822–09 after the glitch of 2007 relative to a simple spin-down model. The observed cubic term points to a large positive second derivative that is explained by the recovery from this glitch.

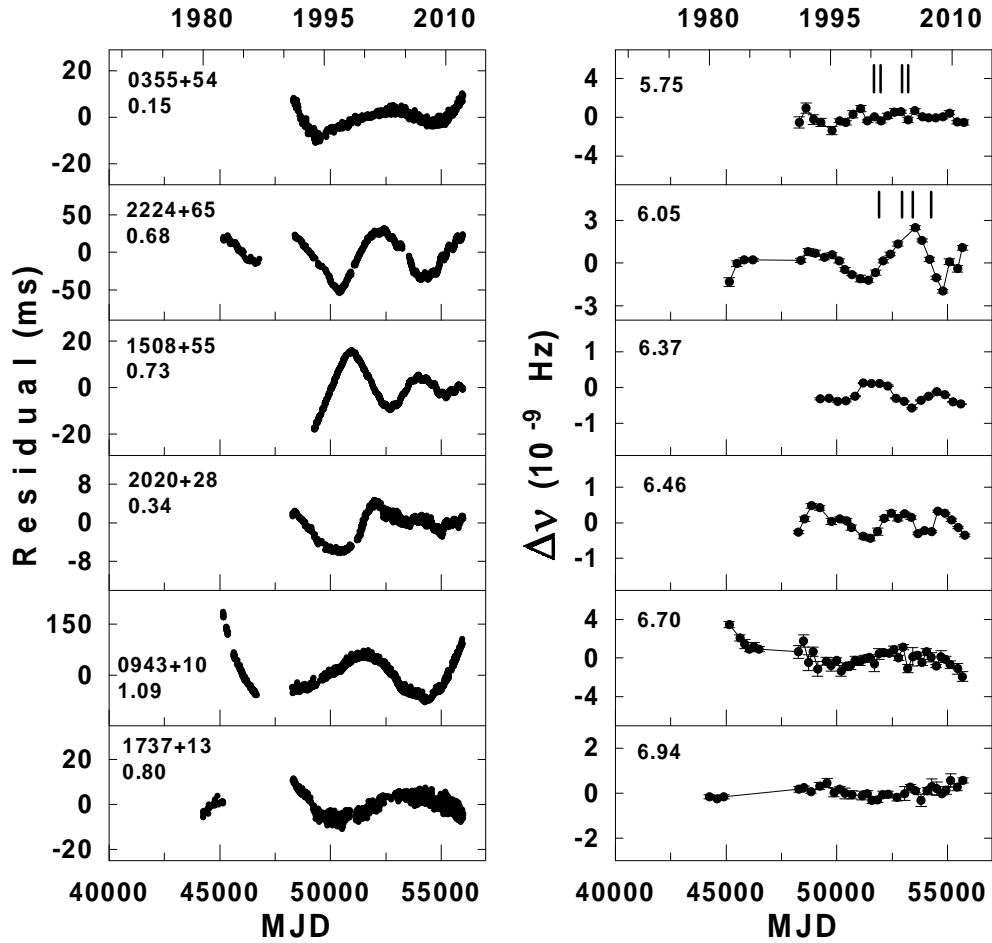


Fig. 8.— Timing and frequency residuals after the removal of a cubic term from the arrival times for the pulsars that show cubic components in their timing residuals. The labels are the same as in Figure 2.

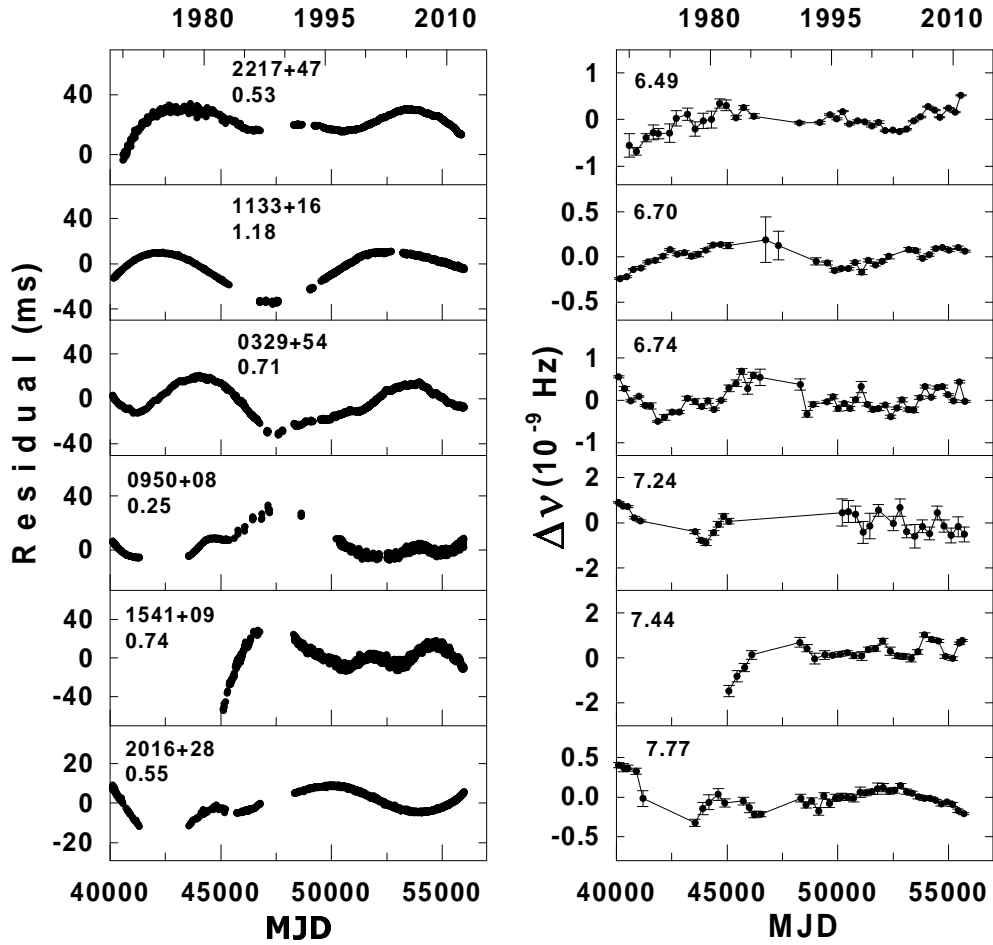


Fig. 9.— Timing and frequency residuals after the removal of a cubic term from the arrival times for the pulsars that show cyclical signatures in their timing residuals. The labels are the same as in Figure 2.

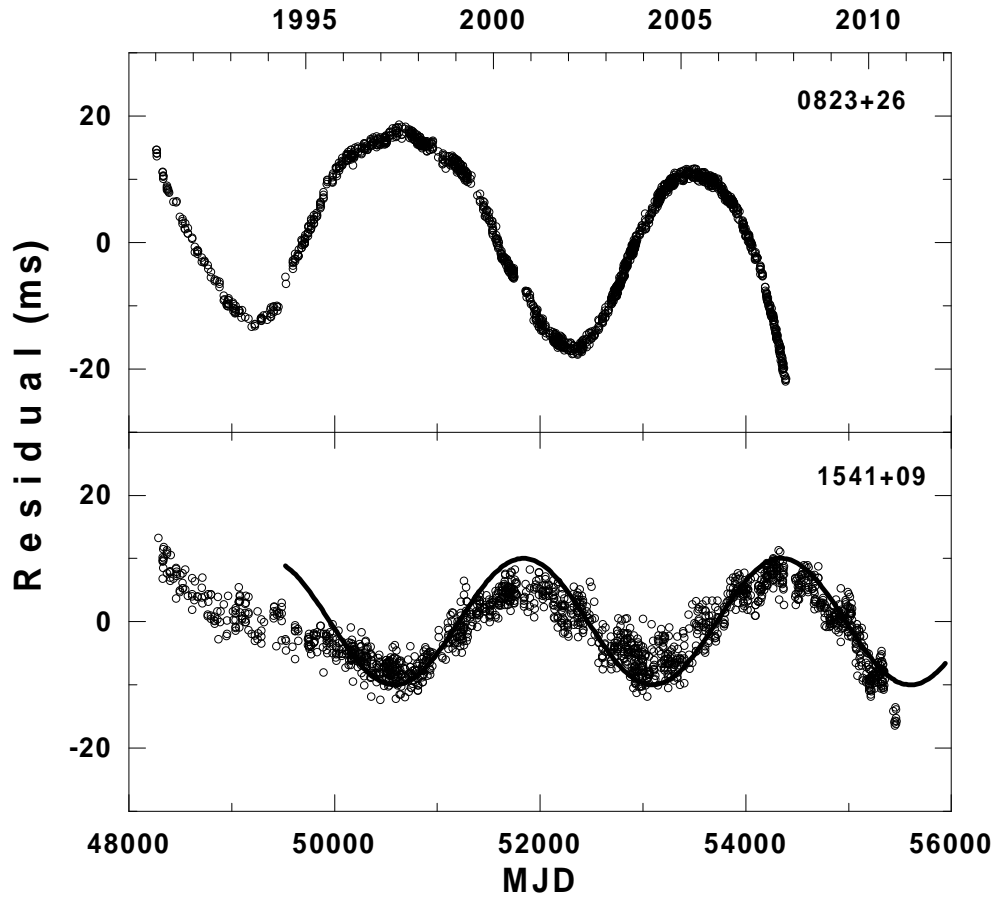


Fig. 10.— Timing residuals for two pulsars, B0823+26 and B1541+09, that exhibit two cycles of clear quasi-sinusoidal structure relative to a simple spin-down model. A sinusoidal function with a period of ~ 7 yr and an amplitude of 10 ms (marked by the bold line) is superimposed on the timing residuals of B1541+09. These quasi-periodic structures are not repeated in further observations.

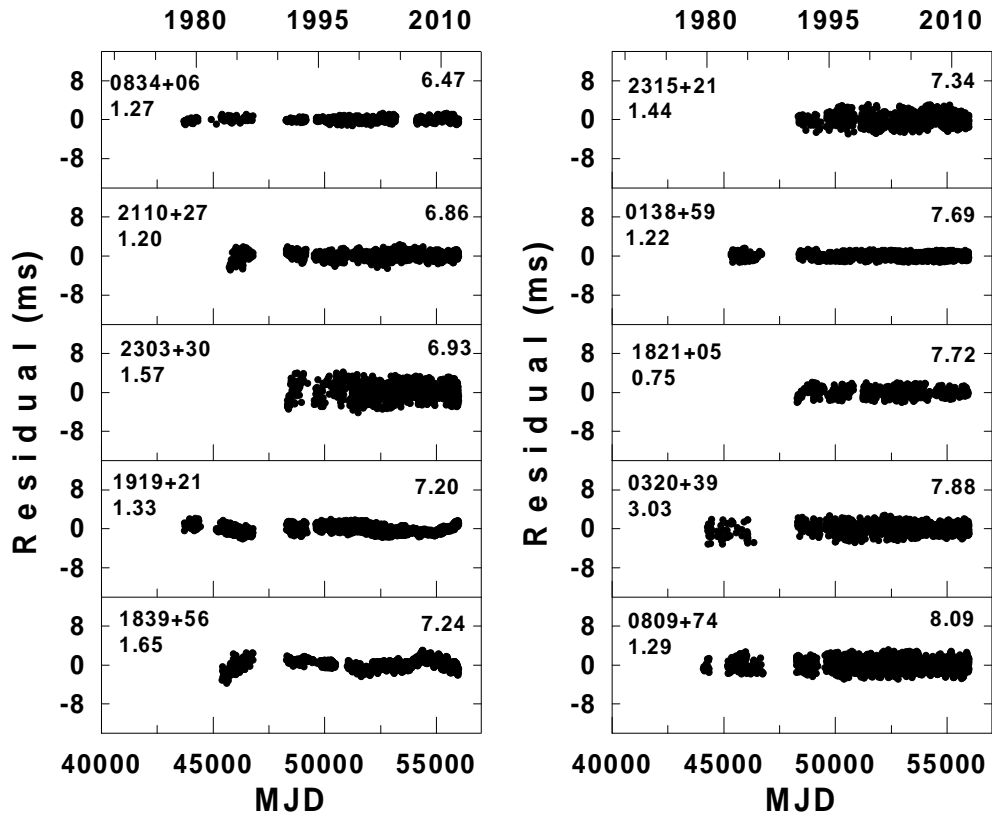


Fig. 11.— Timing residuals after the removal of a cubic term from the arrival times for the pulsars that show noise-like variations in their timing residuals. The labels are the same as in Figure 2.

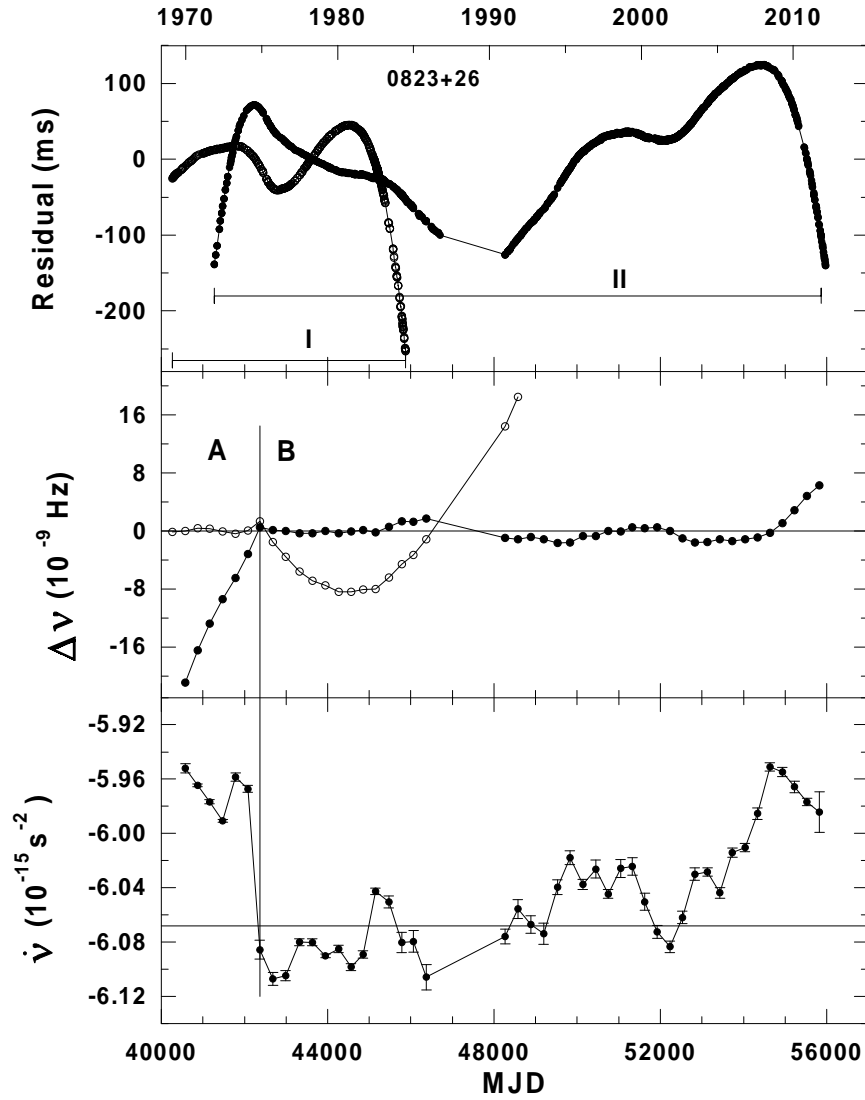


Fig. 12.— Timing behavior of PSR B0823+26 between 1969 and 2012 showing a change in the rotation parameters and a change in the sign of $\ddot{\nu}$. Top panel: the residuals relative to two timing models, including $\ddot{\nu}$ with the opposite signs. The two thin horizontal lines (I and II) indicate the maximum length of each interspace (1969–1984; open circles and 1971–2012; solid circles, respectively), in which the data set can be described by each model within half a pulse period. Middle panel: the $\Delta\nu$ residuals relative to the two ν , $\dot{\nu}$, $\ddot{\nu}$ models: 1969–1974 (section A before the break; open circles) and 1974–2012 (section B after the break; solid circles). The time of the break in $\Delta\nu$ is marked by the vertical line. Bottom panel: $\dot{\nu}$ as a function of time. The break in $\Delta\nu$ produces a distinct jump in $\dot{\nu}$.

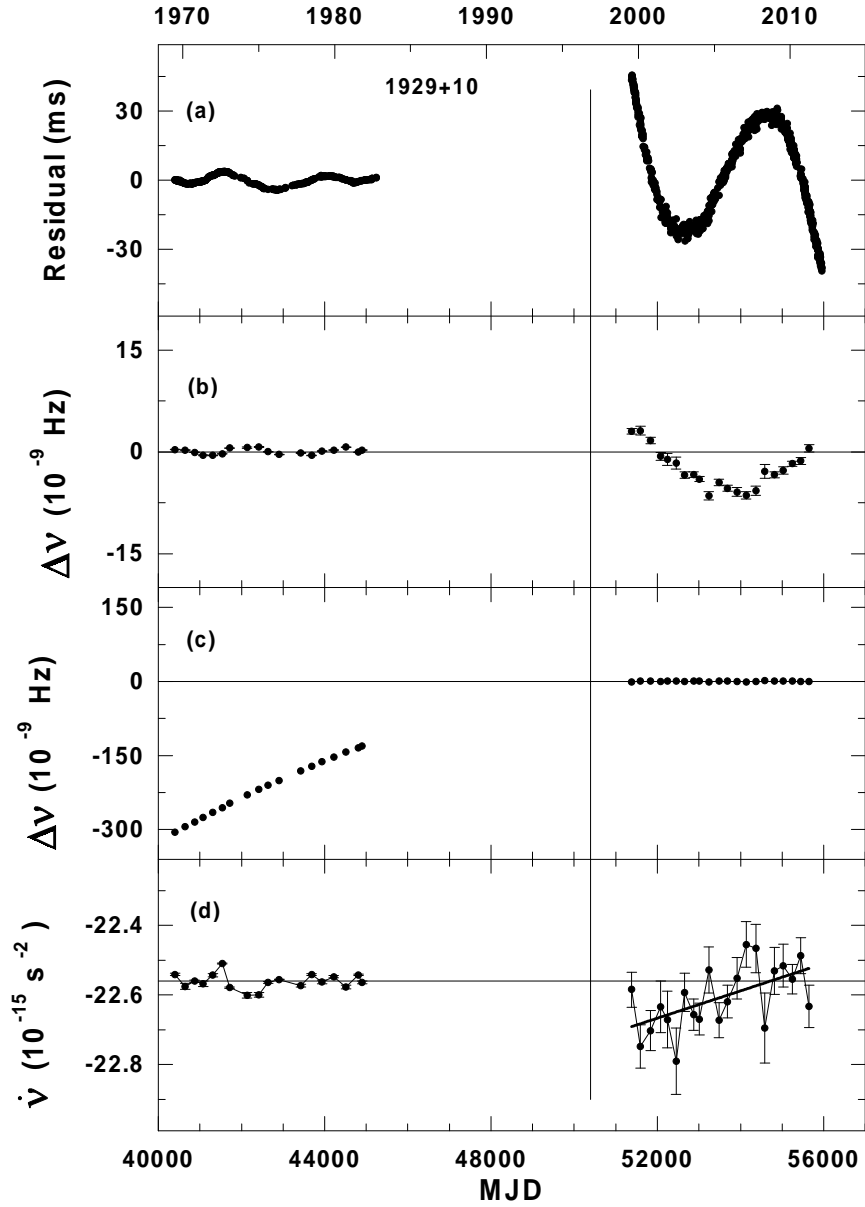


Fig. 13.— Timing behavior of PSR B1929+10 between 1969 and 2012 showing a change in the rotation parameters and a change in the sign of $\ddot{\nu}$. A 16 yr gap in the data is seen between 1982 and 1999. (a) The residuals relative to two simple ν , $\dot{\nu}$ models: 1969–1982 (on the left side) and 1999–2012 (on the right side). The vertical line marks the approximate time of the change of the rotation parameters. (b) The $\Delta\nu$ residuals relative to the ν , $\dot{\nu}$, $\ddot{\nu}$ timing model 1969–1982. (c) The $\Delta\nu$ residuals relative to the ν , $\dot{\nu}$, $\ddot{\nu}$ timing model 1999–2012. (d) $\dot{\nu}$ as a function of time. The best fit linear function is marked by the bold line.

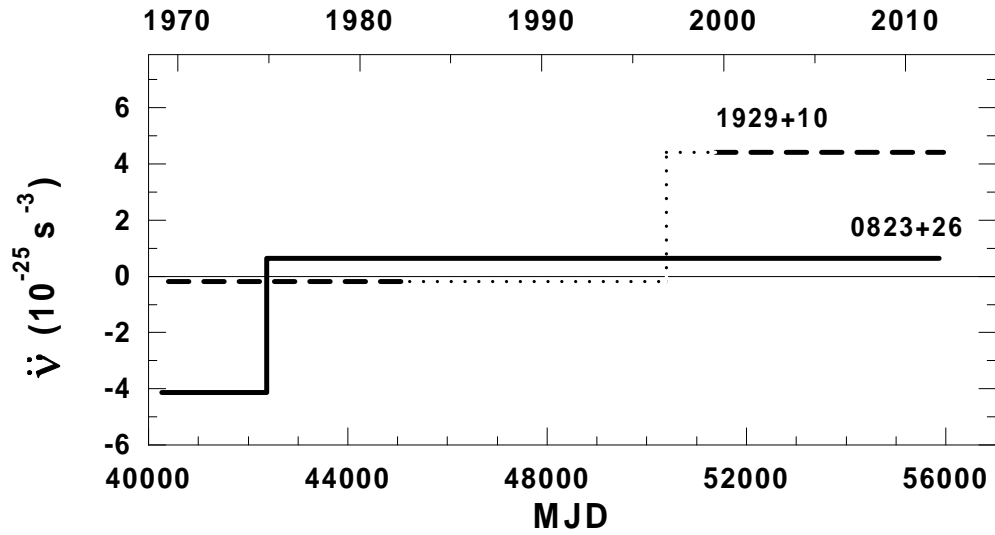


Fig. 14.— Scheme of the time behavior of $\ddot{\nu}$ over the interval 1968–2012 for two pulsars, B0823+26 and B1929+10. The observed change in the value and the sign of $\ddot{\nu}$ is due to a rapid change of the pulsar rotation parameters. We see that the time behavior of $\ddot{\nu}$ for PSR B0823+26 is well described by a rectangular function (the bold line). The behavior of $\ddot{\nu}$ for PSR B1929+10 is plotted by the same function (the dashed line). A 16 yr gap in the data between 1982 and 1999 is marked by the dotted line. The measured values of $\ddot{\nu}$ and the corresponding MJD ranges are taken from Table 2.

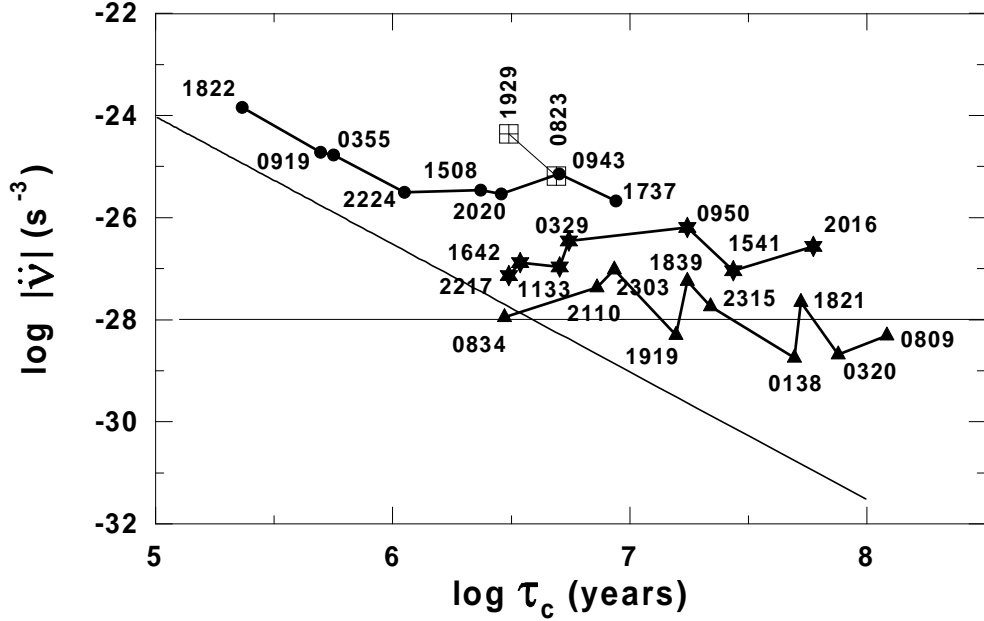


Fig. 15.— Relation between the measured value of $\ddot{\nu}$ and the characteristic age τ_c for 27 studied pulsars. Three groups of pulsars form three sequences that correspond to three types of signatures of the timing residuals. We see that certain signatures of the timing residuals are correlated with certain values of $\ddot{\nu}$ and certain age ranges. The pulsars with residuals dominated by a cubic trend are marked by filled circles, those pulsars with residuals dominated by a quasi-periodic structure are marked by star symbols, and those pulsars with residuals dominated by noise-like variations are marked by triangle symbols. The two pulsars showing a change in the sign of $\ddot{\nu}$ are marked by squares. The thin horizontal line denotes the boundary of accuracy of our measurements, equal to $1 \times 10^{-28} \text{ s}^{-3}$. The thin sloping line shows an evolutionary trend in accordance with a relation $\dot{\nu} \propto -\nu^n$, where $n = 3$.

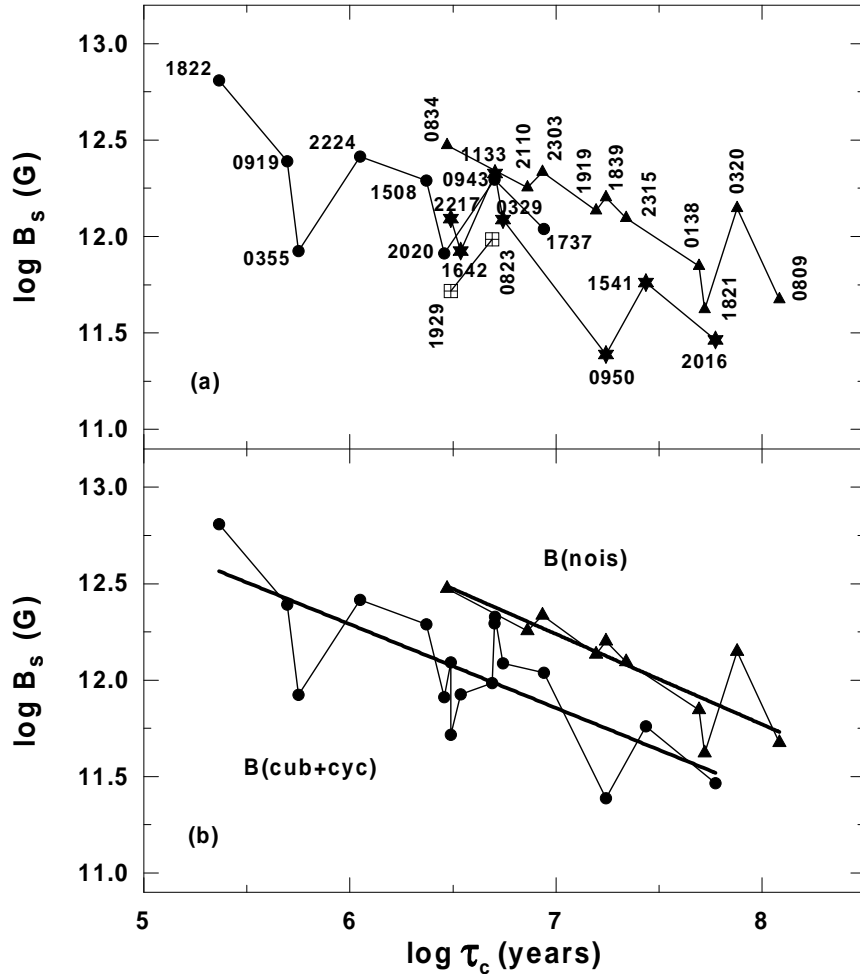


Fig. 16.— Relation between the surface magnetic field strength B_s and the characteristic age τ_c for 27 studied pulsars. (a) The B_s values for the pulsars with cubic signatures in their residuals are marked by solid circles (the B_{cub} values), pulsars with quasi-periodic signatures in their residuals are marked by star symbols (the B_{cyc} values), and pulsars with noise-like signatures in their residuals are marked by triangle symbols (the B_{nois} values). The three plotted sequences indicate that the B_s values are correlated with certain signatures of the timing residuals. (b) The B_s points are plotted as in the top panel (a), but the B_{cub} points and the B_{cyc} points are united in one sequence of the $B_{cub+cyc}$ points marked by solid circles. The two straight lines fitted to the two sequences of the B_s points show that the B_{nois} values are nearly four times greater than the $B_{cub+cyc}$ values for pulsars of the same age.

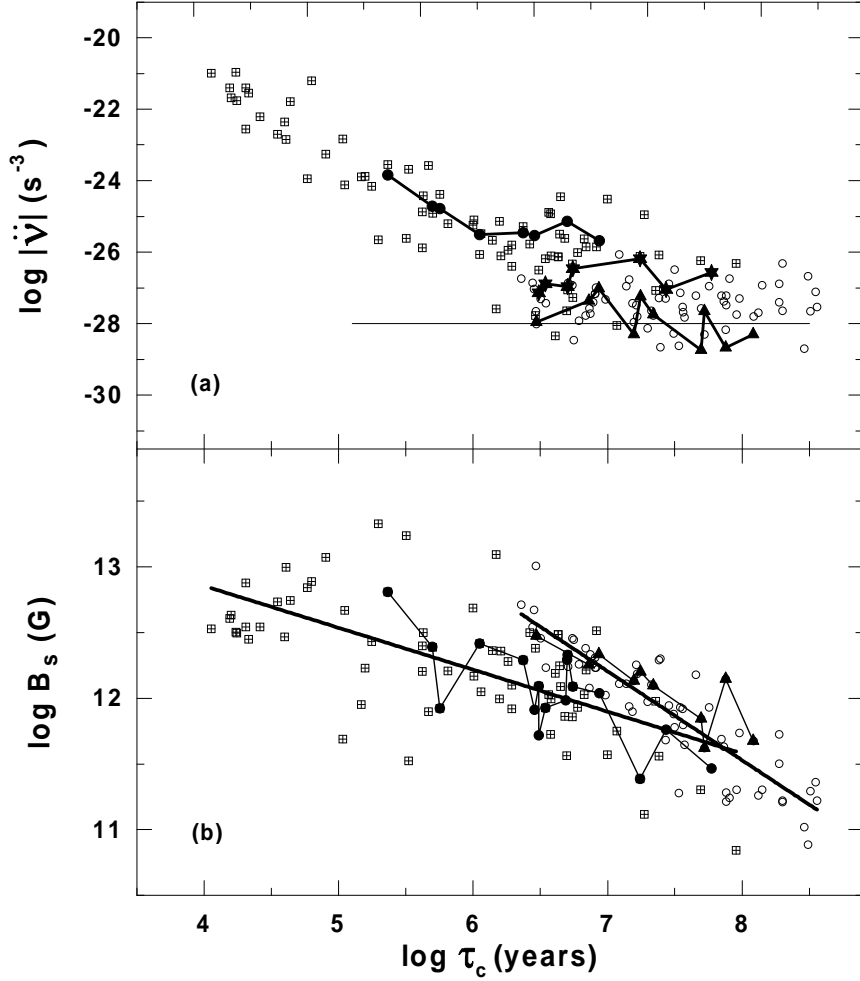


Fig. 17.— Relation between the $\ddot{\nu}$ value, the B_s value, and the characteristic age τ_c for the pulsars from the JBO sample. Here, 73 selected pulsars with cubic or quasi-periodic components in their residuals are marked by squares and 64 pulsars with noise-like components in their residuals are marked by open circles. (a) Relation between the $\ddot{\nu}$ value and τ_c . The three plotted sequences marked by solid lines present the PRAO data, as in Figure 15. We see that the distribution of the JBO points does not contradict the idea of three evolutionary stages in pulsar rotation. (b) Relation between the B_s value and τ_c . The two sequences marked by solid lines show the PRAO data, as in Figure 16(b). The two straight lines fit to two groups of the JBO points show that the magnetic fields are stronger for pulsars exhibiting noise-like signatures in their timing residuals.

Table 1. Information on PRAO Pulse Arrival Time Measurements

PSR J	PSR B	Range (MJD)	No of TOAs	Error (ms)	DM (cm^{-3} pc)	Reference
J0141+6009	B0138+59	45326-55957	1541	0.8	34.91	*
J0323+3944	B0320+39	44268-55973	2660	0.7	26.17	*
J0332+5434	B0329+54	43702-55973	3037	0.05	26.776	1
J0358+5413	B0355+54	45086-55973	2632	0.7	57.153	2
J0814+7429	B0809+74	44087-55973	2777	0.4	5.7513	1
J0826+2637	B0823+26	44807-55973	2706	0.2	19.454	2
J0837+0610	B0834+06	43701-55973	2211	0.1	12.8579	1
J0922+0638	B0919+06	45569-55974	2822	0.5	27.271	2
J0946+0951	B0943+10	45134-55957	1573	0.7	15.4	2
J0953+0755	B0950+08	43703-55958	917	0.2	2.958	2
J1136+1551	B1133+16	46750-55974	2191	0.2	4.8471	1
J1509+5531	B1508+55	49250-55972	2625	0.05	19.613	2
J1543+0929	B1541+09	45088-55972	2723	1.0	34.99	1
J1645–0317	B1642–03	45962-55973	2706	0.3	35.737	*
J1740+1311	B1737+13	48285-55973	1510	1.1	48.673	2
J1823+0550	B1821+05	48284-55950	579	0.9	66.775	2
J1825–0935	B1822–09	48333-55973	1713	1.0	19.383	*
J1840+5640	B1839+56	45398-55973	1743	0.2	26.764	*
J1921+2153	B1919+21	43715-55973	2187	0.2	12.4309	1
J1932+1059	B1929+10	51385-55957	946	0.4	3.180	2
J2018+2839	B2016+28	45724-55973	2327	0.2	14.19	*
J2022+2854	B2020+28	48270-55973	2061	0.4	24.66	*
J2113+2754	B2110+27	45724-55973	2447	0.5	25.113	2
J2219+4754	B2217+47	45073-55973	1491	0.06	43.519	2
J2225+6535	B2224+65	45144-55957	1281	0.8	36.226	*
J2305+3100	B2303+30	48329-55973	955	1.2	49.544	2
J2317+2149	B2315+21	48330-55971	1309	1.1	20.854	*

Note. — In the column order, the table shows the pulsar name (J2000 and B1950), the MJD range of PRAO timing measurements, the number of times of arrival (TOA) in each range, the mean measurement error for observing session lasting from 3 to 11 minutes for different pulsars, and the dispersion measure parameter DM. The references in the last column indicate the DM value that provided the best adjustment between the two sets of the timing residuals obtained for each pulsar at the two observing frequencies of 102.7 MHz (until 1998 May) and 111.3 MHz (since 1998 November) in the PRAO observations.

References. — (1) Taylor et al. (1993); (2) Hobbs et al. (2004); (*) this work.

Table 2. Observed Parameters for 27 Pulsars

PSR B	ν (s ⁻¹)	$\dot{\nu}$ (10 ⁻¹⁵ s ⁻²)	$\ddot{\nu}$ (10 ⁻²⁵ s ⁻³)	Epoch (MJD)	Range (MJD)	σ_2 (ms)	σ_3 (ms)
B0138+59	0.8176959968288(5)	-0.261461(3)	0.00018(6)	45326.7082	45326-55957	0.6	0.5
B0320+39	0.329807506325(1)	-0.069141(3)	0.00021(5)	44268.6762	44268-55973	1.0	1.0
B0329+54	1.399543746342(8)	-4.01374(3)	0.0343(4)	40105.2304	40105-55973	24	11
B0355+54	6.39460122291(2)	-179.7892(2)	1.671(4)	48298.6660	42298-55973	...	2.7
B0809+74	0.773849236501(1)	-0.100671(4)	0.00049(8)	44087.3634	44087-55973	1.2	1.2
B0823+26	1.88444719685(3)	-5.929(1)	-4.14(8)	40264.4381	40264-42364	4.9	1.4
B0823+26	1.88444611497(2)	-6.0976(1)	0.646(2)	42364.6405	42364-55973	...	40.2
B0834+06	0.7850739585879(2)	-4.190673(1)	0.00113(3)	43701.4411	43701-55973	0.3	0.2
B0919+06	2.32226169326(9)	-74.0527(5)	1.91(2)	44210.5817	44210-55139	...	57
B0919+06	2.32219477708(9)	-74.037(5)	18(1)	55140.1604	54140-55974	1.9	2.2
B0943+10	0.91099181885(4)	-2.8750(2)	-0.719(4)	45134.5681	45134-55957	...	48
B0950+08	3.951553316192(9)	-3.58546(3)	-0.0644(6)	40104.8560	40104-55958	20.7	5.1
B1133+16	0.841813872293(3)	-2.64632(1)	0.0109(2)	40154.6631	40154-55974	16	8.6
B1508+55	1.351932973645(13)	-9.13014(9)	-0.347(4)	49250.5223	49250-55972	18	6
B1541+09	1.33609766492(2)	-0.77321(6)	0.009(2)	45087.9517	45088-55972	8.9	8.8
B1642-03	2.57938868630(3)	-11.8466(2)	0.013(3)	40414.1297	40414-55973	23	23
B1737+13	1.245252847252(4)	-2.25742(2)	0.2121(3)	44240.7561	44240-55973	52	4
B1821+05	1.328186108116(4)	-0.40025(2)	0.0022(6)	48284.3024	48284-55950	0.9	0.9
B1822-09	1.30038133415(4)	-88.859(2)	14.4(1)	54116.3366	54116-55973	14.8	4.5
B1839+56	0.6050113973913(7)	-0.547042(3)	-0.0057(2)	45398.2170	45398-55973	2.4	1.0
B1919+21	0.747774504487(1)	-0.753867(2)	-0.00050(5)	43715.8588	43715-55973	0.9	0.8
B1929+10	4.41467924848(3)	-22.5547(4)	-0.18(2)	40401.2136	40401-45236	2.1	2.0
B1929+10	4.41465783839(3)	-22.6674(3)	4.42(1)	51385.8682	51385-55957	20.5	2.3
B2016+28	1.792264372162(6)	-0.47720(2)	0.0269(2)	40105.0491	40105-55973	12.0	4.3
B2020+28	2.912039586312(7)	-16.06542(4)	0.2926(8)	48270.4234	48270-55973	9.6	1.8
B2110+27	0.831358116226(1)	-1.813019(3)	0.00429(7)	45724.4286	45724-55973	1.3	0.7
B2217+47	1.857122692273(8)	-9.53658(3)	-0.0073(3)	40585.0654	40585-55854	7.1	6.1
B2224+65	1.46512685285(5)	-20.7457(2)	0.313(4)	45144.0676	45144-55957	57	24
B2303+30	0.634563570173(2)	-1.16455(2)	-0.0096(5)	48329.3741	48329-55973	2.3	1.7
B2315+21	0.692207715845(1)	-0.501662(8)	-0.0018(3)	48330.3796	48330-55971	1.1	1.1

Table 2—Continued

PSR B	ν (s ⁻¹)	$\dot{\nu}$ (10 ⁻¹⁵ s ⁻²)	$\ddot{\nu}$ (10 ⁻²⁵ s ⁻³)	Epoch (MJD)	Range (MJD)	σ_2 (ms)	σ_3 (ms)
-------	-----------------------------	---	--	----------------	----------------	--------------------	--------------------

Note. — In the column order, the table shows the pulsar’s B1950 name, the pulsar’s rotation parameters ν , $\dot{\nu}$, and $\ddot{\nu}$, the epoch of the ν measurement, the MJD range, the rms value remaining after a second-order fit σ_2 , and the rms value remaining after a third-order fit σ_3 . Numbers in parentheses are 1- σ uncertainties in the last digit quoted. The parameters for B0823+26, B0919+06, and B1929+10 are shown for two timing models at two different intervals.

Table 3. Parameters for Eight Glitches in PSR B1822–09 from the PRAO Measurements

No.	Description of the Glitch	Epoch (MJD)	$\Delta\nu/\nu$ (10^{-9})	$\Delta\dot{\nu}/\dot{\nu}$ (10^{-3})
1	1994	49615(8)	0.2(1)	-0.6(2)
2	1 slow	49857	12.8(2)	-7.0(2)
3	1a slow	50253	4.3(2)	-4.8(3)
4	2 slow	51060	28.7(6)	-24.2(4)
5	3 slow	51879	32.0(9)	-16.7(8)
6	4 slow	52700	2.5(3)	-2.9(3)
7	2006	53745(2)	6.7(4)	-0.1(6)
8	2007	54115.0(2)	121(1)	-0.2(4)

Note. — The table lists the current glitch number, the year for the normal glitch or the number of the slow glitch, the epoch of the normal or slow glitch, and the glitch parameters. Uncertainties in the parameters are in parentheses and refer to the last digit quoted.

Table 4. DM Measurements for PSR B2224+65

DM (pc cm ⁻³)	Epoch (MJD)	Frequencies (MHz)	References
36.16(5)	48382	400, 1640	1
36.079(9)	49303	408, 610, 910, 1630	2
36.226(5)	51100	102.746, 111.646	this work
36.42(2)	52400	840, 1380	3

References. — (1) Arzoumanian et al. (1994); (2) Hobbs et al. (2004); (3) Janssen & Stappers (2006).

Table 5. Glitch Parameters for PSR B2217+47

Glitch Parameters	Values
Pre-glitch parameters	
MJD range	55600–55854
ν (Hz)	1.85711010737(1)
$\dot{\nu}$ (10^{-15} s $^{-2}$)	-9.5599(7)
Epoch (MJD)	55858.0
rms timing residual (μ s)	60
Post-glitch parameters	
MJD range	55866–55973
ν (Hz)	1.85711010972(3)
$\dot{\nu}$ (10^{-15} s $^{-2}$)	-9.536(5)
Epoch (MJD)	55858.0
rms timing residual (μ s)	60
Glitch parameters	
$\Delta\nu/\nu$ (10^{-9})	1.27(4)
$\Delta\dot{\nu}/\dot{\nu}$ (10^{-3})	-2.5(5)
Epoch (MJD)	55858(1)

Note. — The rotation parameters are calculated at the glitch epoch MJD 55858.0.

Table 6. Derived Parameters for 27 Pulsars

PSR B	τ_c (Myr)	$\log(\tau_c)$ (yr)	$\log(\dot{\nu}_{obs})$ (10^{-25} s^{-3})	n	$\log(\dot{\nu}_{exp})$ (10^{-25} s^{-3})	$\log(B_s)$ (G)
B1822–09	0.23	5.36	-23.84	237	-25.74	12.81
B0919+06	0.50	5.70	-24.70	80	-26.15	12.39
B0919+06	0.50	5.70	-23.74	762	-26.15	12.39
B0355+54	0.56	5.75	-24.78	33	-25.82	11.92
B2224+65	1.10	6.05	-25.50	106	-27.06	12.42
B1508+55	2.30	6.37	-25.46	-562	-27.73	12.29
B2020+28	2.87	6.46	-25.53	330	-27.58	11.91
B0834+06	2.95	6.47	-27.96	4	-28.17	12.47
B2217+47	3.08	6.49	-27.14	-14	-27.83	12.09
B1929+10	3.10	6.49	-25.74	-156	-27.46	11.72
B1929+10	3.08	6.49	-24.36	3797	-27.46	11.72
B1642–03	3.45	6.54	-26.89	23	-27.79	11.92
B0823+26	5.04	6.70	-24.38	-22188	-28.25	11.98
B0823+26	4.90	6.69	-25.19	3274	-28.23	11.98
B0943+10	5.02	6.70	-25.14	-7924	-28.56	12.30
B1133+16	5.04	6.70	-26.96	131	-28.60	12.33
B0329+54	5.52	6.74	-26.46	297	-28.46	12.10
B2110+27	7.26	6.86	-27.37	108	-28.93	12.26
B2303+30	8.63	6.93	-27.01	-449	-29.19	12.34
B1737+13	8.74	6.94	-25.67	5181	-28.91	12.04
B1919+21	15.71	7.20	-28.30	-65	-29.64	12.13
B0950+08	17.46	7.24	-26.19	-1979	-29.01	11.39
B1839+56	17.52	7.24	-27.24	-1152	-29.83	12.20
B2315+21	21.86	7.34	-27.74	-496	-29.96	12.10
B1541+09	27.37	7.44	-27.05	2012	-29.87	11.76
B0138+59	49.55	7.69	-28.74	215	-30.60	11.84
B1821+05	52.57	7.72	-27.66	1825	-30.44	11.62
B2016+28	59.50	7.77	-26.57	21186	-30.42	11.46
B0320+39	75.57	7.88	-28.68	1455	-31.36	12.15

Table 6—Continued

PSR B	τ_c (Myr)	$\log(\tau_c)$ (yr)	$\log(\ddot{\nu}_{obs})$ (10^{-25} s^{-3})	n	$\log(\ddot{\nu}_{exp})$ (10^{-25} s^{-3})	$\log(B_s)$ (G)
B0809+74	121.8	8.09	-28.31	3717	-31.41	11.67

Note. — The table lists the pulsars in order of increasing age. The columns list the pulsar B1950 name, the characteristic age $\tau_c = \nu/2\dot{\nu}$ and its logarithmic value, the logarithmic values of the observed value $\ddot{\nu}_{obs}$, the observed braking index $n = \nu\ddot{\nu}_{obs}/\dot{\nu}^2$, the expected value $\ddot{\nu}_{exp} = 3\dot{\nu}^2/\nu$ on a logarithmic scale, and the logarithmic value of surface magnetic field strength $B_s = 3.2 \times 10^{19}(P\dot{P})^{1/2}$ G. The parameters for B0823+26, B0919+06, and B1929+10 are shown for two different models according to Table 2.